

https://dspace.org/

Emerging Pdbased electrocatalysts and supports for ethanol oxidation reaction Highentropy and singleatom materials

Colani Fakude; Aderemi Haruna; Kenneth Ozoemena

ELSEVIER SCIENCE SA
https://hdl.handle.net/10539/41781
SCOPUS

Downloaded from a DSpace repository. https://dspace.org/

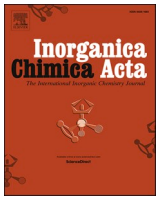
Inorganica Chimica Acta 574 (2025) 122377



Contents lists available at ScienceDirect

Inorganica Chimica Acta

journal homepage: www.elsevier.com/locate/ica



Review article

Emerging Pd-based electrocatalysts and supports for ethanol oxidation reaction: High-entropy and single-atom materials

Colani T. Fakude, Aderemi B. Haruna, Kenneth I. Ozoemena *

Molecular Science Institute, School of Chemistry, University of the Witwatersrand, Johannesburg 2050, South Africa

ARTICLE INFO

Keywords:
Pd-based catalysts
Ethanol oxidation reaction
High-entropy catalysts
Single-atom catalysts
Carbons
MXene

ABSTRACT

Alkaline direct ethanol fuel cells (ADEFCs) offer a promising solution to reduce reliance on fossil fuels. Despite their advantages over hydrogen and methanol fuel cells, the anodic ethanol oxidation reaction (EOR) in ADEFCs faces challenges such as sluggish kinetics and high overpotentials, leading to reduced efficiency. To address these issues, highly active electrocatalysts are essential. This review highlights recent advancements in Pd-based high-entropy materials (HEMs) and single-atom catalysts (SACs) for EOR. Additionally, MXenes, a novel family of two-dimensional materials, have shown promise as supports for these electrocatalysts. We discuss the fundamental principles of EOR, the unique properties of these emerging materials, and their applications in EOR electrocatalysis. Finally, we provide an outlook on future research directions to enhance the commercialization of Pd-based electrocatalysts for ADEFC technologies.

1. Introduction

The provision of affordable, green, and sustainable energy poses a global challenge, and the development of innovative technologies is necessary to pivot away from fossil fuels [1–3]. Fuel cells emerge as a promising solution for mobile power supply, primarily due to their environmental friendliness. Presently, hydrogen, methanol, and ethanol are the main fuels under investigation for fuel cells, each presenting unique advantages and disadvantages, with the choice contingent upon specific requirements. Based on its superior volumetric energy density of 6.28 $kWhL^{-1}$, ethanol emerges as the preferred fuel over H_2 (0.18 $kWhL^{-1}$) and methanol (4.82 $kWhL^{-1}$) [4–6], thus sparking significant interest in alkaline direct ethanol fuel cells (ADEFCs), particularly with the development of anion exchange membranes (AEMs) [7].

In alkaline media, the cathodic oxygen reduction reaction (ORR) has reached a mature stage of development, attributed to its favorable electrokinetics in alkaline electrolytes, making it more conducive for non-noble metals-based electrocatalysts, with FeCo/C being among the simplest of them [8–11]. Electrocatalysts such as FeCo/C combine non-noble metals with readily available carbons like Vulcan carbon, effectively lowering the overall price of the fuel cell. Additionally, the hydroxide anion transport from the cathode to the anode reverses electro-osmotic drag and helps lower ethanol cross-over in the fuel cells, thus reducing the poisoning effect of ORR catalysts. It is also possible to alleviate the issue of voltage drop usually associated with carbonate formation during operations; simply by changing the electrolyte or increasing the operating temperature [12,13]. However, anodic ethanol oxidation experiences sluggish reaction kinetics, meaning the partial oxidation of ethanol to acetate and 4 electrons predominates over the full oxidation to CO_2 and 12 electrons. This necessitates the presence of a proper electrocatalyst for ethanol oxidation reaction (EOR) to occur.

Among the state-of-the-art electrocatalysts, those based on Pd have been tested to be the best, particularly in alkaline media [14,15]. The traditional strategy of alloying Pd with other transition metals is widely recognized as an efficient approach to developing advanced electrocatalysts due to various synergistic mechanisms among the elements incorporated in the alloys such as alloy effect and electronic effects [16]. However, the grand challenge of promoting EOR activity and stability remains unresolved. As a result, the quest for highly effective electrocatalysts and support materials tailored for ethanol oxidation reaction (EOR) is an ongoing focus in this field.

This review aims to provide a brief overview of recent advancements in emerging Pd-based EOR electrocatalysts and support materials. Among the myriad emerging EOR electrocatalysts, high-entropy materials and single-atom catalysts (SACs) are gaining prominence due to their superior performance as EOR electrocatalysts, particularly in cleaving the ethanol C—C bond during the oxidation process. Additionally, MXenes also present themselves as emerging non-carbon

* Corresponding author.
E-mail address: kenneth.ozoemena@wits.ac.za (K.I. Ozoemena).

https://doi.org/10.1016/j.ica.2024.122377
Received 2 June 2024; Received in revised form 9 August 2024; Accepted 10 September 2024
Available online 18 September 2024
0020-1693/© 2024 Published by Elsevier B.V.

supports for EOR. This review begins with an introduction to EOR fundamentals including mechanistic pathways, half-cell testing protocols, and performance metrics including specific activity (SA), mass activity (MA), electrochemical active surface area (ECSA), durability, and Faradaic efficiency (FE). The application of HEMs, SACs, and support materials such as newly developed carbons and Mxenes for pushing the boundaries of catalytic activity for EOR is briefly surveyed. The review then concludes by exploring opportunities, challenges, and prospects associated with these emerging electrocatalysts and support materials.

2. Fundamentals of electrocatalytic ethanol oxidation

The use of ethanol in ADEFCs is based on its remarkable properties, including high theoretical energy density, easy transportability, storage, and non-toxicity. As a means of lowering the carbon footprint, various countries have embarked on producing it on a humongous scale, with the US taking over 50 % of global ethanol production between 2017 and 2021 as indicated in Fig. 1a [3]. The existing ethanol supply chains and its ease of production make ethanol an even more sustainable fuel choice. Ethanol can be extracted from crops such as beetroot and sugarcane *via* fermentation processes as well inedible parts of food plants or biomass resources such as grass, poplar, and forest residue, as well through the catalytic reaction of ethene with steam makes the use of ethanol sustainable than the other fuels [17,18].

The oxidation of ethanol can occur in either acidic or alkaline environments, and the reaction mechanism under these conditions remains the same. However, the downside of low-pH environments is their general corrosiveness, which may negatively impact the stability of electrocatalysts. In contrast, alkaline fuel cells benefit from abundant OH^- ions that can adsorb on electrocatalytic surfaces to form OH_{ads} without water dissociation, facilitating the oxidation of intermediates and resulting in facile electrokinetics than in acidic environments [20]. The generally facile electrokinetics allows for the use of non-Pt electrocatalysts such as Pd, as well as non-noble, cheap, and readily available co-electrocatalysts such as Ni, Fe, Co, Mg, etc [21–23]. Consequently, proton exchange membranes (PEM) are unsuitable for alkaline media due to low H^+ concentrations which may cause sluggish kinetics. Instead, anion exchange membranes (AEMs), which allow anion exchange from the anode to the cathode are preferably employed [7].

2.1. EOR mechanism in alkaline media

Pioneering studies into the EOR mechanism emerged during the 1950 s, eventually progressing into a dual pathway referred to as the C1 and *C*2 pathways. Although early research on DEFCs commenced in acidic environments, it was subsequently discovered that the kinetics of cleaving the resilient C—C bond during the oxidation process are significantly hindered in acidic electrolytes [24]. Cui *et al.* [25] employed density functional theory (DFT) calculations to demonstrate that the dehydrogenation of ethanol, is hindered by the absence of OH species for prompt removal of adsorbed hydrogen (H_{ads}). This deficiency ultimately impedes the electrooxidation process. Thus, alkaline conditions based on sodium hydroxide (NaOH) and potassium hydroxide (KOH) were proposed. Amongst these two, KOH emerged as a preferred electrolyte due to its less corrosive nature, high conductivity, and ability to reduce Ohmic overpotential better than NaOH [26].

The release of the total chemical energy in ethanol is attainable *via* the C1 pathway where 12 electrons are released. This pathway commences with the chemisorption of ethanol in the initial stages followed by consecutive dehydrogenation steps to produce $CH_3CH_2O^-$/CH_3CHO_{ad}/CH_3CHO_{ad} intermediates [27–29], which may undergo C—C bond cleavage into C1 species (CH_x and CO) and can be oxidized into CO_3^{2-} or CO_2 as a final product (C1 pathway, Fig. 1b) or directly oxidized into acetate (CH_3COO^-) without further oxidation (*C*2 pathway) [30]. The oxidation of CHO_{ad} (and other C1 species such as

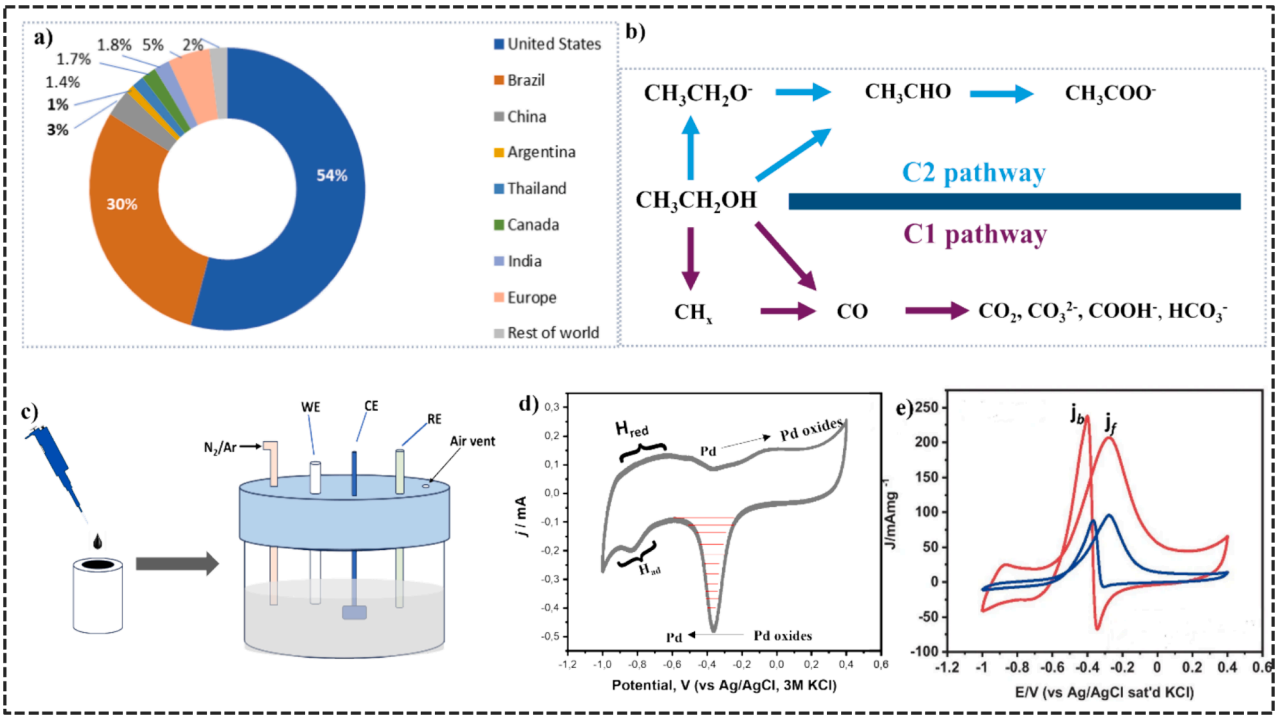


Fig. 1. a) Chart showing predictions of worldwide bioethanol production by country [18], **b)** EOR parallel pathways [19], **c)** Schematic: glassy carbon electrode drop-casting technique, and a typical three-electrode set-up for ethanol electrooxidation experiment, **d)** Typical cyclic voltammetry curves for determining the electrochemical surface area on Pd-based electrocatalysts. The oxygen desorption region (shown by the arrow in the negative scan) is utilized for determining the electrochemically active surface area by integrating the PdO reduction peak (area marked by red lines). H-adsorption and H-reduction peaks are poorly defined for Pd-based electrocatalysts and thus may not be suitable for ECSA calculations. **e)** Typical EOR CV where current is normalized by electrocatalytic loading.

CH_x a) may also undergo direct and indirect pathways in the early stages of the oxidation process, accompanied by the production of CO_{ad} which can be further oxidized to CO_2 or carbonate.

In the *C*2 pathway, the C—C bond is not broken, especially in low-temperature fuel cells. In this pathway, the partial oxidation of ethanol releases only 2 to 4 electrons, inevitably leading to the release of only ~ 36 % of chemical energy from ethanol [29]. It is worth mentioning that the inertness of the C—C bond is brought about by the high activation energy (87.3 kcal/mol) of C—C bond cleavage and the orientation of ethanol's atoms which sterically hinders the C—C bond [26]. Moreover, amongst the possible intermediates,CO_{ad} is the most stable, blocking the active sites, and preventing the proceeding of EOR at low potentials. At first, Pt was regarded as the benchmark electrocatalyst to drive the EOR process, but research in the last three decades Pd has emerged as a catalyst of choice, particularly in alkaline media. The main reason for this is that Pt is more prone to catalytic deactivation due to easy poisoning by the CO intermediate, while, on the upside, Pd is more electrocatalytically stable, more geologically abundant (fifty times more abundant than Pt), and demonstrates high electrocatalytic activity, particularly in alkaline media resulting to satisfactory power densities of up to 170 $mWcm^{-2}$ at relatively high potentials [2,25]. However, a major drawback of Pd-based electrocatalysts lies in their tendency to selectively oxidize ethanol to acetate ions in highly alkaline environments. Consequently, each ethanol molecule can only yield a maximum of four electrons, rather than the theoretically possible twelve electrons from complete oxidation to carbonate resulting in low Faradaic efficiency (FE). While this low FE can be compensated by the generally facile electrokinetics for improved power densities, Pd-based electrocatalysts exhibit a second drawback at potentials values of 0.6 V vs reversible hydrogen electrode (RHE) in half cells and 0.15 V vs RHE in monoplanar DEFCs, in that surface adsorbed Pd - OH_{ads} species (Eq.1) active for the oxidation of ethanol, begin to convert to inactive Pd-O following Eq.2 and Eq.3 [31]. This results in the reduction of active sites and ultimately slows down or inhibits the ethanol oxidation process.

$$Pd + OH^- \rightarrow Pd\text{-}OH_{ads} + e^- \quad [1]$$

$$Pd\text{-}OH_{ads} + OH^- \rightarrow Pd\text{-}O + H_2O + e^- \quad [2]$$

$$Pd\text{-}OH_{ads} + OH^- \rightarrow Pd\text{-}O + H_2O + e^- \quad [3]$$

In as much as it has been reported that the Pd oxidation to Pd-O on the DEFC anodes can be minimized by the addition of small amounts of $NaBH_4$ into the anolyte compartment to reduce Pd-O to Pd [32], the design of effective EOR electrocatalysts, particularly those that can oxidize Pd^0 to Pd - OH_{ads} to facilitate a continuous EOR process remains imperative.

2.2. Fabrication protocols and performance metrics

A full fuel cell test of a given catalyst *via* MEA is a complicated and quite a tedious process, usually complicated by various engineering factors in the design of the MEA. The MEA comprises of three major compartments: electrode supports (i.e. anode and cathode), electrolyte, and electrocatalysts [7]. The main purpose of electrocatalysts, particularly the anode catalysts, is to provide a surface for the anodic oxidation of ethanol to occur at lower activation energy, extended duration, and improve the reaction rate [33]. However, a full cell test of a given electrocatalyst *via* MEA is associated with tedious and time-consuming steps owing to various complicated engineering factors in the MEA. Therefore, a simple alternative for rapidly screening and evaluating the EOR electrocatalyst typically relies on half-cell experiments conducted in three-electrode systems, usually composed of Pt, Ag/AgCl glassy carbon as a counter (CE), reference (RE), and the working electrode (WE), where a Luggin capillary is preferably used to separate the CE and RE to avoid cross-contamination by chlorine anions [30]. The electrocatalyst is typically homogenously dispersed in a proper solvent (e.g. isopropanol + H_2O, ethanol, plus Nafion as a binder), and deposited on the WE surface. Catalyst deposition can be done *via* drop-casting as indicated in Fig. 1c [4], electrodeposition, or physical vapor deposition [30,34]. The electrocatalyst loading can be determined before loading using inductively coupled plasma optical emission spectroscopy (ICP-OES). Prior to electrochemical measurements, the electrolytes (e.g. 1 M KOH, 0.5 H_2SO_4, or $HClO_4$) are purged with N_2 or Ar to remove dissolved O_2 and other contaminants, helping maintain stable and clean electrode surfaces, which is crucial for accurate and reproducible measurements. The loaded electrocatalysts are typically first activated by carrying out consecutive cyclic voltammetric (CV) scans under the Ar/N_2 purged electrolytes to obtain stable CV curves. For the electrochemical active surface area (ECSA), the electrocatalysts are scanned at a lower scan rate. To determine the efficiency of an electrocatalyst, while maintaining lower noble metal loading with improved fuel utilization efficiency in fuel cell devices, the following parameters are very essential: electrochemical surface area (ECSA), specific activity (SA), mass activity (MA), Onset potential (E_{onset}), j_f/j_r ratio, Faradaic efficiency, and durability.

2.2.1. Critical parameters for evaluating EOR

ECSA, SA, MA, and E_{onset}.

The electrochemical surface area (ECSA) is a crucial parameter for directly determining the catalyst utilization efficiency. A larger surface area typically exposes more active sites where reactions can occur. For Pd-based electrocatalysts, the ECSA can be determined *via* the oxygen desorption region by integrating the PdO reduction peak and working out the area according to Eq. (4).

$$ECSA_{PdO} = \frac{Q}{SI} \quad [4]$$

where Q is the Coulombic charge, S is the charge required to reduce monolayer Pd (0.424 mCm^{-2}), and *I* ($mgcm^{-2}$) is the electrocatalytic loading. The determination of ECSA using this method conveniently avoids complications of using poorly defined hydrogen peaks associated with Pd (see Fig. 1d), or surface contamination observed with other methods such as C_{upd} and CO stripping [35,36]. More importantly, the ECSA parameter serves to represent the activity for a single active site and thus reflects the intrinsic electrocatalytic activity of an electrocatalyst [21]. SA can be defined as the oxidation forward peak current (j_f) normalized by the ECSA. The SA of electrocatalysts can be typically determined by catalyst active sites such as electronic and local coordination environments and these can be tailored by engineering ligand environment [37], lattice strain [38], controlling the exposed facets [39], etc. On the other hand, MA refers to the oxidation forward current (j_f) normalized by the electrocatalytic mass loading (see Fig. 1e) [40]. It can also be obtained as a product of SA and ECSA and thus can be boosted by improving both the ECSA and SA. This parameter is crucial in that it reveals the mass of the noble metal required to achieve a particular current output [30]. E_{onset} is generally the potential at which the EOR initiates and generates a measurable current. This parameter is essential for indicating the ease of the EOR electrocatalysis process, i.e. the more negative the value, the easier the electrocatalysis [41].

The controversial j_f/j_r ratio.

The j_f peak indicates the oxidation of freshly chemisorbed ethanol while j_b has been suggested to represent the oxidation of residual intermediates [42]. Following the work by Lui and co-workers [42], the j_f/j_b ratio is used to describe a catalyst's ability to tolerate poisoning by the carbonaceous species. Under this interpretation, a higher ratio indicates a sufficient ethanol oxidation process during the forward scan, with few carbonaceous residues left, thus suggesting a high EOR electrocatalysis process [34,41,43]. However, investigations by Hofstead-Duffy and colleagues showed through a series of *in situ* surface-enhanced IR adsorption spectroscopic (SEIRAS) experiments that the j_f/j_b empirical

criterion is not appropriate for gauging the CO-tolerance and catalytic activity of electrocatalysts and, thus no longer suitable for this purpose [44]. Instead, CO stripping experiments are highly recommended to understand the CO tolerance of any electrocatalyst better [45].

Faradaic efficiency.

Faradaic efficiency (FE) refers to the ratio of the actual amount of a desired product generated during an electrochemical reaction to the theoretical amount that could be produced based on Faraday's law. In the context of EOR the key desired product in a complete oxidation process is CO_2, while acetate is a significant product when incomplete oxidation occurs. FE is calculated as a ratio of the experiment charge (Q) to the theoretical charge ($Q_{theoretical}$) required to produce the measured amount of CO_2. Based on Faraday's law of electrolysis, the theoretical charge is expressed as [16];

$$Q_{theoretical} = znF \quad [5]$$

where *z* is the theoretical number of electrons to form the CO_2 product, *n* is the number of moles produced, and F is the Faradaic constant (~96485 $Cmol^{-1}$). Thus, FE can be expressed as a % as indicated in Eq. (6).

$$FE(\%) = \frac{Q_{theoretical}}{Q} \times 100\% \quad [6]$$

However, it is worth mentioning that owing to the difficulty in cleaving the C—C bond in the C1 pathway, EOR often involves the *C*2 pathway which produces acetate with only 4-electron transfer, which greatly lowers the utilization efficiency of ethanol (~36 % utilization fuel efficiency). In this respect, the identification and quantification of the possible by-products are critical for evaluating the selectivity of the *C*2 pathway to quantify the FE and understand the reaction mechanism, which often requires multiple analytical approaches, including the ion chromatography [46], nuclear magnetic resonance (^{1}H NMR) [46], *in situ* IR [47,48], and differential electrochemical-mass spectrometry (DEMS) [47].

Durability.

The durability of electrocatalysts is crucial for assessing their electrocatalytic efficiency in practical applications. Over extended electrocatalytic experiments conducted under harsh electrochemical conditions, electrocatalysts may undergo an Oswald ripening process or aggregation, resulting size increase. This increase in particle size can eventually destabilize the electrocatalyst, leading to detachment from electrode surfaces. Moreover, catalysts' active sites may also be susceptible to attack or blockage by undesired hydroxides, causing a reduction in the apparent surface area (SA) and electrochemically active surface area (ECSA) [49,50]. On the other hand, Pd-based electrocatalysts may also be poisoned by carbonaceous species such as CO over extended operations [4]. To characterize the electrocatalyst's durability, two methods are widely employed: chronoamperometry (CA) and CV cycling stability measurements, carried out in a mixture of ethanol and KOH. CA evaluates current drop at a fixed potential, while for cycling measurements, CV curves are recorded over extended periods (usually hundreds, thousands, or even more), to check the oxidative current decay by comparing the initial and the last CV scans [51]. Observations during EOR stability tests using CA have shown current drops of over 70 % within the first hour while they can perform hundreds of cycles without obvious current decay using CV [52–57]. This can be attributed to the removal of toxic species at high potential regions during CV scans but will accumulate during CA tests. Therefore, since DEFCs are operated at specific potentials in practical applications, it becomes more reasonable to evaluate long-term durability tests using CA [58].

3. Emerging EOR electrocatalysts

Conducting the EOR process in alkaline media has opened the possibility of utilizing non-noble metals, lowering the production cost of DEFCs [4]. Although Pt-based electrocatalysts employed in acidic environments may be adaptable to alkaline conditions, Pd-based electrocatalysts exhibit superior efficacy owing to their higher oxophilicity and comparatively inert characteristics [59]. Pure Pd when used alone may be highly susceptible to poisoning by notorious intermediates such as CO, limiting their stability and durability. Alloying Pd with one or more oxophilic metals such as Ni, Sn, Mn, Fe [14,59,60], metal oxides such Ni $(OH)_2$ [4], SnO_2 [57], CeO_2 [6], etc, is the most traditional method of improving EOR activity. The alloying process can improve the electrocatalytic process by synergism and increase lattice strain. This ultimately alters the electronic environment of Pd, altering its *d*-band center and affecting the adsorption of intermediates in favor of improved EOR electrocatalysis. On the other hand, oxides are known to promote the adsorption of OH (OH_{ads}) at lower potentials to transform CO-like intermediates on Pd surfaces to CO_2 or other products releasing blocked active sites for further electrochemical reaction [61]. As an upgrade to traditional mono, bimetallic, and trimetallic Pd-based electrocatalysts, high entropy materials are attracting immense research interest for EOR electrocatalysis [40,62–66].

3.1. Pd-based high-entropy materials

Recent advancements in the field of electrocatalysis have highlighted the significant potential of high-entropy materials (HEMs) in enhancing catalytic performance [64,65,67,68]. Traditional low-entropy (1–2 metals) and medium-entropy (3–4 metals) catalysts, although effective, often face limitations such as poisoning by reaction intermediates and suboptimal stability under extreme conditions. HEMs offer a promising alternative due to their unique structural and compositional characteristics. High-entropy materials (HEMs) represent a new class of materials e.g. high-entropy alloys (HEA), with attractive electrocatalytic properties. As opposed to the traditional low entropy and medium entropy electrocatalysts, HEMs are flexible and inclusive, typically composed of five or more elements uniformly mixed to form solid solutions and exhibit enhanced configurational entropy (S), as given by Eq. (7), which imparts remarkable stability and catalytic activity [69].

$$\Delta S_{mix} = -R\left(\frac{1}{n}\ln\frac{1}{n} + \ln\frac{1}{n} + \ln\frac{1}{n} + \ldots\ldots + \frac{1}{n}\ln\frac{1}{n}\right) = -R\ln\frac{1}{n} = R\ln n \quad [7]$$

where *n* is the number of elements, and R is the molar gas constant such that for a material with five elements, the expression becomes $\Delta S_{mix} = R\ln 5 \approx 1.61R$, but there is no maximum number of elements in HEMs [69–72]. The synergistic effects of multiple elements provide different adsorption sides, facilitating optimal adsorption of reaction intermediates to achieve ideal reaction rates [73]. HEMs also exhibit excellent catalytic stability, thanks to the entropic and hysteresis diffusion effects, rendering them highly resilient under extreme reaction conditions such as high/low-temperature conditions and strong acidic/alkaline electrolytes [74].

The distinct physical and chemical properties, including excellent electrochemical properties of HEMs, originate from the following four effects indicated in Fig. 2:

- *high-entropy*- is associated with confining multiple atomic species into the same lattice to the benefit of the formation of stable single-phase solid-solution structures rather than fragile intermetallic compounds [68,75];
- *lattice distortion*- is formed due to the large difference in the atomic sizes of the elements comprising the HEM;
- *Sluggish diffusion*- this effect is closely linked to lattice distortion in the sense that severe lattice distortion raises the energy barrier of atomic diffusion within the HEM sub-lattice endowing stability to the material [76];

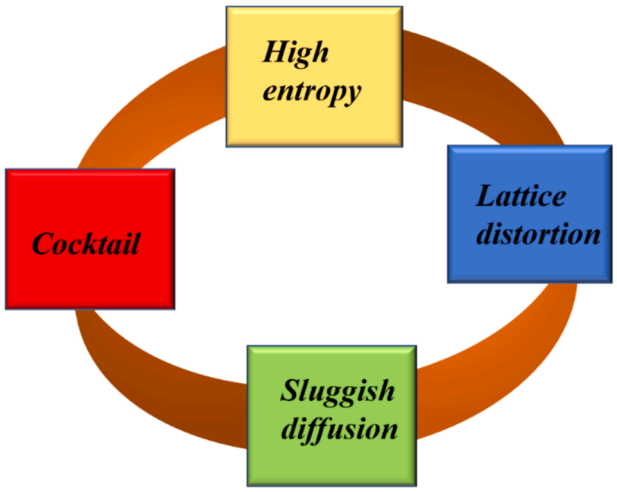


Fig. 2. Core effects in HEMs.

- *"cocktail" effect*- means that the synergistic response among the various element components in the HEM gives rise to various unique properties [77,78].

HEMs can be subdivided into high-entropy alloys (HEAs) and high-entropy ceramics (HECs). HEAs are composed solely of metallic compounds whereas HECs can include non-metallic groups. HECs encompass a variety of materials including high-entropy oxides [70,72,79], high-entropy borides [80,81], high-entropy sulfides [82], high-entropy silicides [83], high-entropy nitrides [84], high-entropy fluorides [85] amongst others. Amongst these HEMs, HEAs are the ones predominantly applied in ADEFCs.

Low-entropy and medium-entropy Pd-based electrocatalysts are prone to poisoning by intermediate products such as CO, resulting in reduced selectivity for C1 products during EOR oxidation. The incorporation of more elements to form high-entropy material electrocatalysts is an effective approach to mitigate this issue. It is worth mentioning that when designing HEMs for EOR electrocatalysis, it is crucial to incorporate Pd (including Pt) as the most active site for EOR. Other studies introduce active sites such as Rh, Os, etc., to facilitate C—C bond cleavage, and Ru is employed as an active site for oxidizing reaction intermediates. The composition of HEMs is adjusted to modify the coordination environment of the active sites, aiming to tailor the adsorption energy of ethanol and its intermediates at these sites, for enhanced EOR activity. To develop economically viable ADEFCs, while maintaining or improving the overall efficiency, low-cost elements such as Ni, Fe, Mn, etc are usually incorporated. This allows the interaction between the components to modify the electronic structure of the Pd/Pt active centers, shift their *d*-band center, and facilitate the optimal bonding of the electrocatalyst with CO,CH_x,CH_3CO^{-}, acetaldehyde (C_2H_4O), among others. This interaction can also influence the bonding of the electrocatalysts with the OH_{ads} to promote the oxidative removal of CO [63]. As an example, abundant and low-cost Fe, Ni, Co, and Mn, based on their ability to easily form solid solutions with Pd/Pt, were used to rationally design a septenary HEA composed of Pt, Pd, Fe, Co, Ni, Sn, and Mn (denoted as PtPd HEA). The elements demonstrated entangled electronic and synergistic effects in the HEA. These carefully selected elements maximized the utilization of precious Pt and Pd metals while leveraging the beneficial properties of the low-cost, more abundant Fe, Co, Ni, Sn, and Mn to attain a 17 times more EOR activity for the PtPd HEA electrocatalyst that commercial Pt/C. First-principle calculations using DFT revealed that Fe, Co, and Mn prevent Pt and Pd sites from reacting with water to form Pt/Pd-OH*, which would otherwise hinder the EOR process. While Ni and Sn were both found to enhance CO tolerance, Ni lowered the EOR activation barrier, while Sn promoted C—C cleavage [16].

Lao *et al* [86] reported an *fcc*-structured Pd-enriched-HEA-core and Pt-enriched-HEA-shell NPs (PdAgSn/PtBi HEA NPs) prepared by a simple low-temperature method. The material possessed many active sites and enhanced Pd (and Pt) sites thanks to their unique coordination environment. DFT studies revealed that Pt sites exhibited a positive *d*-band center while Pd sites employed a relatively positive *d*-band center relative to the Fermi level, where the former enhanced OH* adsorption, but the latter decreased CO* adsorption. Moreover, the cascade C1 and *C*2 reactions were promoted by various binding groups closely linked to the various element-based sites at optimal binding energies. Electrochemical studies revealed that the PdAgSn/PtBi HEA NPs exhibited EOR mass activity of 3386 $mAmg^{-1}_{(Pd+Pt)}$ which was 5.4 and 4.9 times higher than those of the commercial Pd/C and Pt/C counterparts (Fig. 3a). DFT calculations were performed and Fig. 3b shows the step-by-step oxidation of the α-C atom of ethanol to CH_3COOH *via* the *C*2 pathway (R_1-R_7) and CO_2 (R_1-R_6) *via* the C1 pathway with *C*2-pathway dominating. The DFT predictions indicated that EOR is more favorable on the Pd sites compared to the Pt sites because of the relatively unstable adsorption of C1/*C*2 intermediates (such as CO* and CH_3*) on the Pd site, which is associated with more negative *d*-band value relative to the Fermi level.

Stability, as revealed by long-term CV tests, shows that the as-synthesized HEM maintained EOR mass activity of 47.5 % MA after 500 potential cycles. Post-mortem analysis indicated that the PdAgSn/PtBi HEA NPs kept the *fcc* structure with limited compositional changes. In another study, Li *et al* [87] alloyed immiscible elements into a quaternary alloy with 98 % Al to form a precursor AlPdNiCuMo high-entropy alloy, which was later de-alloyed by electrochemical cycling in 0.5 M H_2SO_4. The de-alloying process removed a portion of Al, Ni, Cu, and Mo and XPS spectra showed that after cycling in the acid, the intensity of Pd became stronger with peak shifting to higher binding energy levels, indicating a highly exposed Pd on the surface, accompanied by a downshift in the *d*-band center, resulting in enhanced EOR activity. The HEA exhibited a mass activity of 2.67 A mg^{-1}_{Pd}. A two-electrode flexible cell solid-state ethanol fuel cell was then assembled, and it delivered an energy density of 13.63 $mWhcm^{-2}$ with just 3 mL ethanol (Fig. 4a), which is remarkable when compared with other solid-state energy devices. XRD and STEM results showed that the structural integrity of HEA nanoparticles was maintained after a long-term operation (0.5 $mAcm^{-2}$) without any microstructure coarsening.

Given that Pd is a highly active site for EOR, it remains critically important to expose Pd-active sites on catalyst surfaces. In this context, Zeng *et al* [88], reported a surface-decorated FeCoNiSn non-noble HEA as a core and decorated its surface with Pd to form an NHEA@NHEA-Pd core–shell (see Fig. 4b). The non-noble FeCoNiSn provided a high-entropy coordination environment in the sense that they were spatially distributed around the catalytically active Pd site and thus altered its electronic environment for enhanced performance.

Indeed, the NHEA@NHEA-Pd core–shell demonstrated high electrocatalytic activity for EOR with an MA of 7.34 A mg^{-1}_{Pd}, high stability (>91.8 % retention after 2000 cycles), and excellent CO tolerance. This work demonstrates the critical role of high-entropy coordination and morphological control in HEA catalysts toward improved activity, and stability, at a significantly reduced cost. In situ surface-enhanced infrared absorption spectroscopy (SEIRAS) investigation provided insights into the electronic structure of the NHEA@NHEA-Pd and Sn@Sn-Pd high-entropy alloy catalysts during the electrocatalytic reaction. The spectra obtained from SEIRAS indicated that Pd atoms in the high-entropy alloy catalysts are in a unique electronic state different from those of bulk Pd and that they interacted with the neighboring alloying elements. Moreover, the results showed that the addition of Sn or NHEA onto the Pd surface increases its catalytic activity. This implies that high-entropy alloy catalysts have unique electronic, chemical, and structural properties that contribute to their catalytic activity, highlighting their potential as effective electrochemical catalysts.

In another study, Wu and co-workers [40] combined all the PGMs *via*

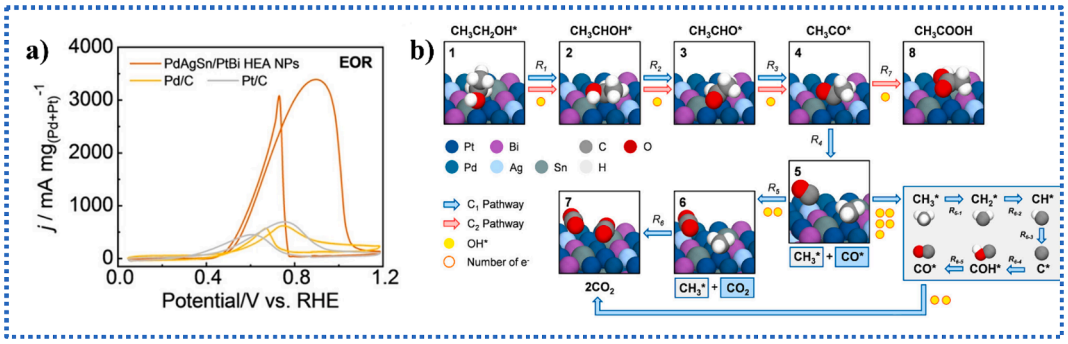


Fig. 3. **a)** CV polarization for EOR on PdAgSn/PtBi HEA Nps, Pd and Pt, **b)** DFT calculation: scheme of intermediate and major products involved in EOR, Reprinted with Ref. [86] Copyright (2023) Wiley-VCH GmbH.

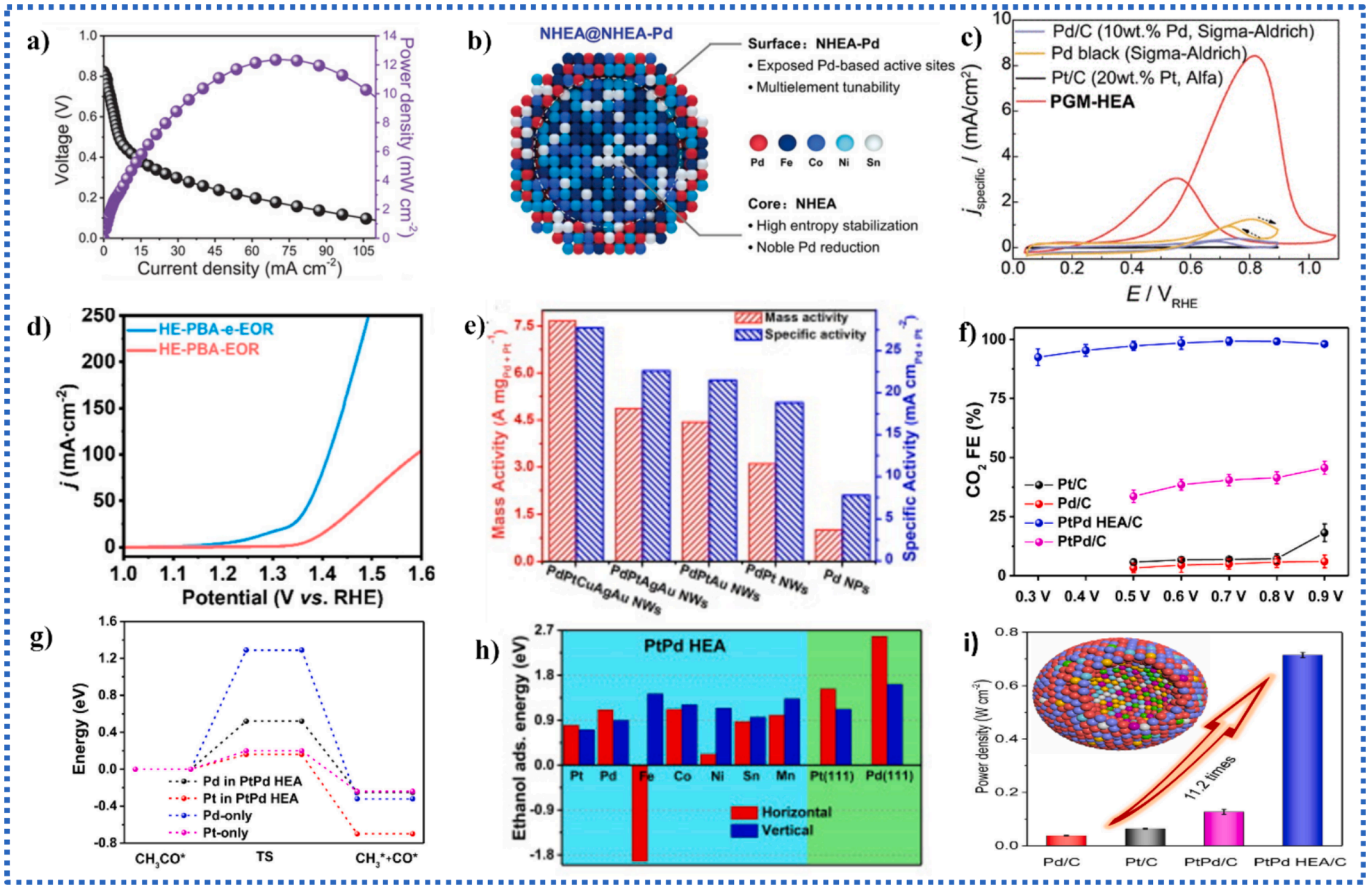


Fig. 4. **a)** LSV profile and the power densities at different current densities. Reprinted from Ref. [87], with permission from ACS, Copyright (2023). **b)** The scheme of NHEA@NHEA-Pd catalyst, Reprinted from Ref. [88], with permission from Wiley-VCH GmbH, Copyright (2022), **c)** CV profiles of PGM-HEA compared to commercial electrocatalysts for EOR, Reprinted with permission from Ref. [40], Copyright (2020) ACS. **d)** EOR performance of HE-PBA-e compared to HE-PBA toward EOR, Reprinted from Ref. [89] with Permission from ACS, Copyright (2023). **e)** Summarized mass/specific activities of PdPtCuAgAu HEA NWs against other electrocatalysts. Reprinted from Ref. [90], with permission from Elsevier, Copyright (2022). **f)** Faradaic efficiency of complete EOR at different potentials for Pt/Pd HEA electrocatalyst, **g)** DFT calculated reaction energy barrier of C—C cleavage on Pt and Pd sites on the PtPd HEA, compared with pure Pt, and Pd based on Pd/Pd (111) facets, **h)** EOR adsorption energy with the horizontal and vertical direction of all elements in PtPd HEA, Pt (111), and Pd (111) facets **i)** Power density of Pt/Pd HEA/C compared to Pd/C, Pt/C and PtPd/C (inset: model of Pt/Pd HEA). Reprinted from Ref. [16], with permission from Elsevier, copyright (2023).

a facile wet chemical method to synthesize RuRhPdOsIrPt HEA (PGM-HEA) nanoparticles based on the premise that PGMs possess various active sites ideal for the catalysis of complex reactions involving several reactants and intermediates. CV tests proved that the PGM-HEA effectively catalyzed the EOR process to the delivery of 12 electrons exhibiting MA(SA) 2.5 (3.2), 6.1 (9.7), and 12.8 (3.4) higher than commercial Pd/C, Pd black and Pt/C at 0.45 V, respectively (Fig. 4c). The PGA-HEA even outperformed Au@PtIr/C, an electrocatalyst known for the highest EOR performance ever recorded. Additionally, the PGM-HEA showed remarkable stability towards EOR. For confirmation, gas detectors indicated that more CO_2 was released than CO for the PGM-HEA, indicating higher selectivity for the C1 pathway as compared to commercial Pd/C.

Prussian blue analogs (PBAs), represent a class of perovskite-type materials whose application is yet to gain ground in electrocatalysis. On this basis, Xu *et al* [89], utilized simple co-precipitation of four metal

cations (i.e.,Co^{2+}, Zn^{2+}, Cu^{2+}, and Ni^{2+}) and $K_3[Fe(CN)_6]$, followed by $NH_3{\cdot}H_2O$ etching to fabricate high-entropy Prussian blue analogs (HE-PBA-e) for EOR. Compared to the non-etched counterpart, HE-PBA-e exhibited remarkable ECSA and rich nano-pores for boosted electron transfer and mass transport. Moreover, HE-PBA-e possessed a high concentration of high oxidation state of metals believed to be the real active species for the electrooxidation of ethanol. Thus, HE-BPA-e achieved a current density of ~ 250 $mAcm^{-2}$ while HE-BPA delivered 50 $mAcm^{-2}$ (at 1.5 V *vs* RHE), as indicated in Fig. 4d with respective Tafel slopes of 144 $mVdec^{-1}$ and 576.1 $mVdec^{-1}$, demonstrating high activity and high EOR kinetics on the HE-BPA-e electrocatalyst. In another study, Fan *et al* [90] reported on the synthesis of PdPtCuAgAu HEA nanowires (NW) using one using a one-pot strategy with the help of a carboxylic N-(carboxymethyl)-N,*N*-dimethylhexadecane-1-aminium bromide (C_{16}N-COOH(Br^-)) as a structure directing agent. The C_{16}N-COOH(Br^-) surfactant was selected based on the ability of Br- to rapidly exchange with $PdCl_4$ to form $PdBr_4$ which can facilitate mild Pd reduction at lower redox potential, which is favorable for the growth of the nanowire morphology. PdPtCuAg, PdPtAuAg, and PdPtCuAu, PdPtAu, bimetallic PdPt, and monometallic Pd NW network were also synthesized using following the same procedure for comparison purposes. PdPtCuAgAu HEA NWs exhibited excellent electrocatalytic activity (Fig. 4e) than the other catalysts, thanks to its structural anisotropy which boosted the mass activity *via* improved electron/mass transfer and enhanced the catalyst utilization efficiency. Upon conduction chronoamperometry of 5000 s, the PdPtCuAgAu HEA NW electrocatalyst maintained its original morphology, indicating high stability and high CO tolerance. The authors attributed the high performance of the electrocatalyst to the four core effects i.e. high-entropy, lattice distortion for high mass activity, sluggish diffusion, and cocktail effects for poisoning resistance.

An exceptionally performing HEM for EOR electrocatalyst was reported by Chang and co-workers [16]. The authors used solvothermal synthesis to meticulously develop a septenary PtPdFeCoNiSnMn (PtPd HEA) electrocatalyst for ethanol oxidation reaction (EOR), incorporating Pt, Pd, and non-noble metals Fe, Co, Ni, Sn, and Mn. This electrocatalyst features a Pt/Pd-rich surface but an ultra-low loading of platinum group metals (PGM). After elucidating and proving the role of each element in the PtPd HEA, the non-PGM metals were found to play an active role in stimulating the EOR activity of Pt and Pd active centers. Fe, Co, and Mn adsorbed water and made the Pd and Pt clean and ready for EOR. The PtPd HEA demonstrated FE>92 % for complete ethanol oxidation on a wide potential range as illustrated in Fig. 4f. The two key competing reactions toward complete EOR are referred to as C—O coupling and C—C cleavage of the CH_3CO^* intermediate as indicated in Eqs. (8 and 9), respectively [91]:

$$CH_3CO* + OH* \rightarrow CH_3COOH* + * \quad [8]$$

$$CH_3CO* + * \rightarrow CH_3* + CO* \quad [9]$$

Theoretical studies of EOR on Pt(111) and Pd(111) surfaces of Pt/Pd HEA reveal that the reaction barrier for C—C cleavage was lower for the HEA than for Pt and Pd alone (see Fig. 4g). DFT calculation further revealed different ethanol adsorption strengths at various metal sites on HEA surfaces, as well as on Pt(111) and Pd(111), in both horizontal and vertical configurations (Fig. 4h). Calculations showed that ethanol binds more strongly on pure metal surfaces compared to the HEA surface, which makes it difficult for the products of EOR to desorb, leading to blocked active sites. The adsorption strength decreased from 2.58 and 1.53 eV on the Pd(111) and Pt(111) surfaces, respectively, to 1.11 and 0.80 eV on the Pd and Pt sites of PtPd HEA as indicated in Fig. 4h. The addition of non-PGM elements resulted in a suitable adsorption strength for ethanol on the Pt and Pd sites of PtPd HEA. Ethanol adsorption on Pt and Pd slightly favors horizontal configurations, while Co, Ni, Sn, and Mn prefer vertical configurations. On the Fe site, ethanol dissociates into OH* and C_2H_4* horizontally, but vertically, it adsorbs with the highest energy. For most other sites, the difference in adsorption strengths between configurations is minimal (<30 meV). Thus, the presence of multiple adsorption sites with similar energies is advantageous for ethanol adsorption and oxidation. Therefore, ethanol is expected to first adsorb on non-PGM elements, with nearby Pt and Pd facilitating thorough oxidation on the PtPd HEA. After demonstrating negligible (0.01 % and 0.03 % respectively) EOR performance decay after 30 000 and 50 000 cycles, respectively, the assembled DEFCs using Pt/Pd HEA obtained a maximum power density of 0.72 Wcm^{-2} and a durable operation for 1,200 h, which was higher than that of commercial electrocatalysts for DEFCs as indicated in Fig. 4i. The authors concluded that the PtPdHEA/C electrocatalysts shows great promise for practical application, particularly in solving the storage and transportation issues associated with H_2 fuel cells.

The results of EOR electrocatalysis by the Pd-based HEMs are tabulated in Table 1. It is worth noting that the EOR performance demonstrated by these materials is commendable and promising for practical applications. It is also demonstrated that these materials can maintain enhanced activity for a long period, indicating outstanding electrochemical durability and stability with the PtPdFeCoNiSnMn HEA being the most stable EOR electrocatalyst (Fig. 5). The excellent electrochemical activity of HEMs is based on the rational design where elements are carefully selected to maximize the utilization of precious metal Pd (including Pt) while leveraging their beneficial properties such as low cost and abundance. As a result, detailed mechanism studies reveal that most HEMs can catalyze the EOR process in a 12-electron process, which suggests a great potential for HEMs to drive the complete oxidation of ethanol.

4. Pd-based single-atom electrocatalysts

It is worth mentioning that despite the unique abilility of HEMs to stabilize multiple elements in a single-phase structure, resulting to exceptional features such as enhanced catalytic performance and stability, there is room for improvement. Active sites in HEMs are often part of a complex, multi-element matrix, potentially hampering the catalytic efficiency. In contrast, single atom catalysts (SACs) provide a more efficient catalytic environment offering isolated, highly active sites, leading to superior catalytic performance, especially in reactions like EOR. This is because it has been well established that the size of nanoparticles has a significant effect on their catalytic performance. So, it is well expected that tuning the structure of an electrocatalyst at an atomic level and decreasing the size of the metal nanocluster could be key in maximizing the efficiency of atomic utilization for improving electrocatalytic performances [92]. However, the surface free energy of metals significantly increases with particle size decrease, leading to unwanted aggregation. To circumvent this, appropriate support materials that strongly interact with SACs provide stabilization to prevent the aggregation process and thus form finely dispersed metal clusters. Xu and colleagues demonstrated that it is possible to to combine the merits of HEMs and SACs, where HEMs would act as support structures for SACs [85]. The authors demonstrated this possibility by stabilizing Pd SACs onto high-entropy fluorite oxides, $(CeZrHfTiLa)O_x$, creating what they termed Pd@HEFO. This can be an avenue worth exploring for EOR to take advantage of the synergies between SACs and HEMs.

The transition from bulk complexity of HEMs to atomistic precision of SACs opens a new avenue for engineering catalysts with unprecedented performance and stability. In this context, it is paramount to understand that the genesis of the 'single atom catalysis' concept traces back to the pioneering studies by Zhang and co-workers in 2011 [93,94]. The authors reported Pt SACs stabilized on a FeOx support for the synthesis of Pt/FeOx electrocatalyst which was both highly active and stable for CO oxidation. They proposed that the presence of more vacant *d*-orbitals, owing to electron transfer from Pt to the FeOx support, was responsible for the extraordinary binding and stabilization of the single Pt atoms. The positively charged Pt accounted for the superb catalytic

Table 1
Pd-based HEMs as electrocatalysts for ethanol oxidation in alkaline environments.

HEM electrocatalyst	Synthesis method	Observed properties	Electrochemistry	Stability	Refs.
PdAgSn/PtBi HEA	Low-temperature method	Pd-rich core and Pt-rich shell with highly exposed active sites.	Mass activity of 3386 $mAmg^{-1}_{(Pd+Pt)}$,	Activity retention of 54.6 % after 7200 s CA and 47.5 % after 500 CVs.	[86]
NHEA@NHEA-Pd	Two-step thermal shock process	FeCoNiSn core, with Pd atomically dispersed on the shell. High Pd utilization efficiency.	E_{onset} of 0.37 V, Mass activity of 7340 $mAmg^{-1}_{Pd}$, specific activity of 6.20 $mAcm^{-2}$	Activity retention of 98.8 % after 2000 CVs	[88]
PGM-HEA	Polyol method	Intrinsically possess various active sites with high stability	Mass activity of 1 600 $mAmg^{-1}_{Pd}$	–	[40]
AlPdNiCuMo HEA	Precursor alloy design and chemical dealloying	Hierarchical nanoporous structure	Mass activity of 2 670 $mAmg^{-1}_{Pd}$, 13.63 $mWhcm^{-2}$ with 3 mL ethanol, discharge durability of ~ 120 hr.	–	[87]
HE-PBA-e	Co-precipitation and etching	High concentration of high oxidation state of metals, and rich nano-pores.	Current density ~ 250 $mAcm^{-2}$@ 1.5 V(*vs* RHE), Tafel slope of 144 $mVdec^{-1}$.	–	[89]
PdPtCuAgAu HEA NWs	One-pot synthesis method	Well-dispersed nanowire with average diameter ~ 3.5 nm	Mass activity of 7.7 $Amg^{-1}_{(Pd+Pt)}$,	Activity retention of 60 % after 500 CVs	[90]
PtPdFeCoNiSnMn HEA	Solvothermal synthesis	PtPd rich surface, average diameter ~ 0.65 nm, homogenous distribution of elements	E_{onset} of 0.255 V_{RHE}, Mass activity of 24.3 Amg^{-1}_{PGMs} at 0.815 V $_{RHE}$, Power density of 0.72 Wcm^{-2}@ 1.3 Acm^{-2}, stability of 1200 h (50 days)	Activity retention of 99.99 % after 30 000 CVs and 99.97 % after 50 000 CVs,	[16]

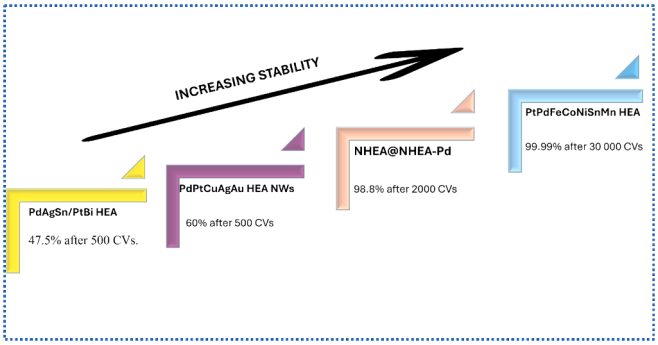


Fig. 5. Flow chart showing the percentage current density retained after a specific number of voltammetry cycles during EOR using HEMs.

activity. Since then, SACs have continued to garner much attention in recent years, arousing great interest in heterogeneous catalysis [95–99].

To further show that heterogenous catalysis with SACs is no longer a dream, various SACs have been fabricated and applied for EOR. For example, Pei *et al.* [54], outlined an approach of rationally designing a multi-metallic catalyst comprising of multiple active sites consisting of Pd nanoclusters and Ru single atoms anchored on the defective sites of $Ni(OH)_2$, as shown in Fig. 6a. The authors based their approach on the fact that metal hydroxides SACs can offer ample adsorbed hydroxyl (OH_{ads}) species, which are suggested to aid in the oxidative elimination of CO from Pd surfaces through the Langmuir-Hinshelwoood mechanism and thus improve EOR stability. The $Pd_{12}Ru_3/Ni(OH)_2/C$ electrocatalyst attained higher electrocatalytic activity (3.724 A mg^{-1}_{PdRu}) compared to the other electrocatalysts (Fig. 6b and c). $Ni(OH)_2$ coordinated to Ru facilitated the oxidative removal of reaction intermediates, thereby improving the stability of the $Pd_{12}Ru_3/Ni(OH)_2/C$ material. Electrochemical *in situ* FTIR measurements indicated improved selectivity for CO_2 production by the $Pd_{12}Ru_3/Ni(OH)_2/C$ electrocatalyst, indicating the role of the tri-component synergy of Pd, Ru, and $Ni(OH)_2$: Ru single atoms provide improved adsorption of OH*, Pd clusters adsorb ethanol, and the OH* expedites the oxidative elimination of reaction intermediates (i.e. CO_{ad}, CH_3COO_{ad} etc).

A similar study was conducted by Li *et al.* [100], where they reported on a hybrid catalyst consisting of Pd nanoparticles uniformly dispersed on a carbon framework-supported Ni SACs to form Pd NPs@Ni SAC for EOR, as indicated in Fig. 6d. TEM showed Pd nanoparticles with an average size between 2 to 5 nm (Fig. 6e), while HR-TEM showed lattice fringes of (1 1 1) with a *d*-spacing of 0.224 nm (Fig. 6f), demonstrating high crystallinity. The authors confirmed the presence of Ni-OH bonds using XPS, EXAFs, and XANES where Ni SACs were well dispersed on the carbon support through Ni-OH and Ni-O coordination. The Pd NPs@Ni SAC material obtained superb MA of 1093 mA mg^{-1}_{Pd} at 0.92 V, exceeding that of Pd NPs@Cu SAC and Pd NPs@C at 965 and 787 mA mg^{-1}_{Pd}, respectively, as illustrated in Fig. 6g. Thanks to the facile oxidative removal of reaction intermediates, the electrocatalyst exhibited high electrocatalytic stability and high Faradaic efficiency (Fig. 6j).

Metallenes have emerged as materials with great potential in electrocatalysis. Metallene are 2D materials exhibiting expansive lateral dimensions, abundant active sites, and superior electronic conductivity. Combining metallenes with single-atom doping is appealing, especially if they are assembled into 3D nanostructures to form nanomaterial aerogels. In this way, the properties of metallenes (e.g., high electrical conductivity, excellent catalytic activities, and special plasmonic behavior) and those of aerogels (e.g., self-supported feature, continuous porous structure, and superior specific surface area) are synergized to fabricate better electrocatalysts. On this premise, Wang, and co-workers [101] intelligently doped Pd metallene aerogels (Pd MAs) with W single-atoms to create SA W-Pd MAs. The authors followed a bubbling CO-induced gelation method in acetic acid at 50 ℃, as indicated in Fig. 7a, to obtain hierarchical nanoporous metallene Pd structure and single-atom W-doped electrocatalysts with high activity and selectivity for C1 EOR process. The W-doping facilitated an excellent EOR yielding an MA of 5.29 A mg^{-1}_{Pd} and SA of 10.9 mA cm^{-2} (Fig. 7b) which are respectively 3.1 and 1.4 and 2.3 and 1.3 times higher SA than both commercial Pd/C and Pd/C. The EIS plot in Fig. 7c shows that SA W-Pd MAs has facile electrokinetics than the commercial counterparts. *In situ* FTIR and 1H NMR analysis demonstrated high selectivity of the C1 pathway, and DFT calculations indicated that the SA W-Pd MAs had its *d*-band center shifted by 0.06 eV relative to Pd as illustrated in Fig. 7d, suggesting that the W single atoms altered the electronic structure of surface Pd. This alteration caused a reduction in the adsorption energies of reaction intermediates and thus explains excellent EOR catalysis that favors the C1 reaction pathway.

As part of an ongoing endeavor to address the problem of poor stability of SACs, the prospect of utilizing metal frameworks as supports emerges as a promising strategy for enhancing the stability of SACs in electrocatalytic contexts. This approach is predicated on the establishment of strong metal–metal bonds that can tune the electronic environment of active sites and optimize the binding strength with reaction intermediates for improved electrocatalytic activity and stability. The class of SACs born from this interaction are referred to as single atom

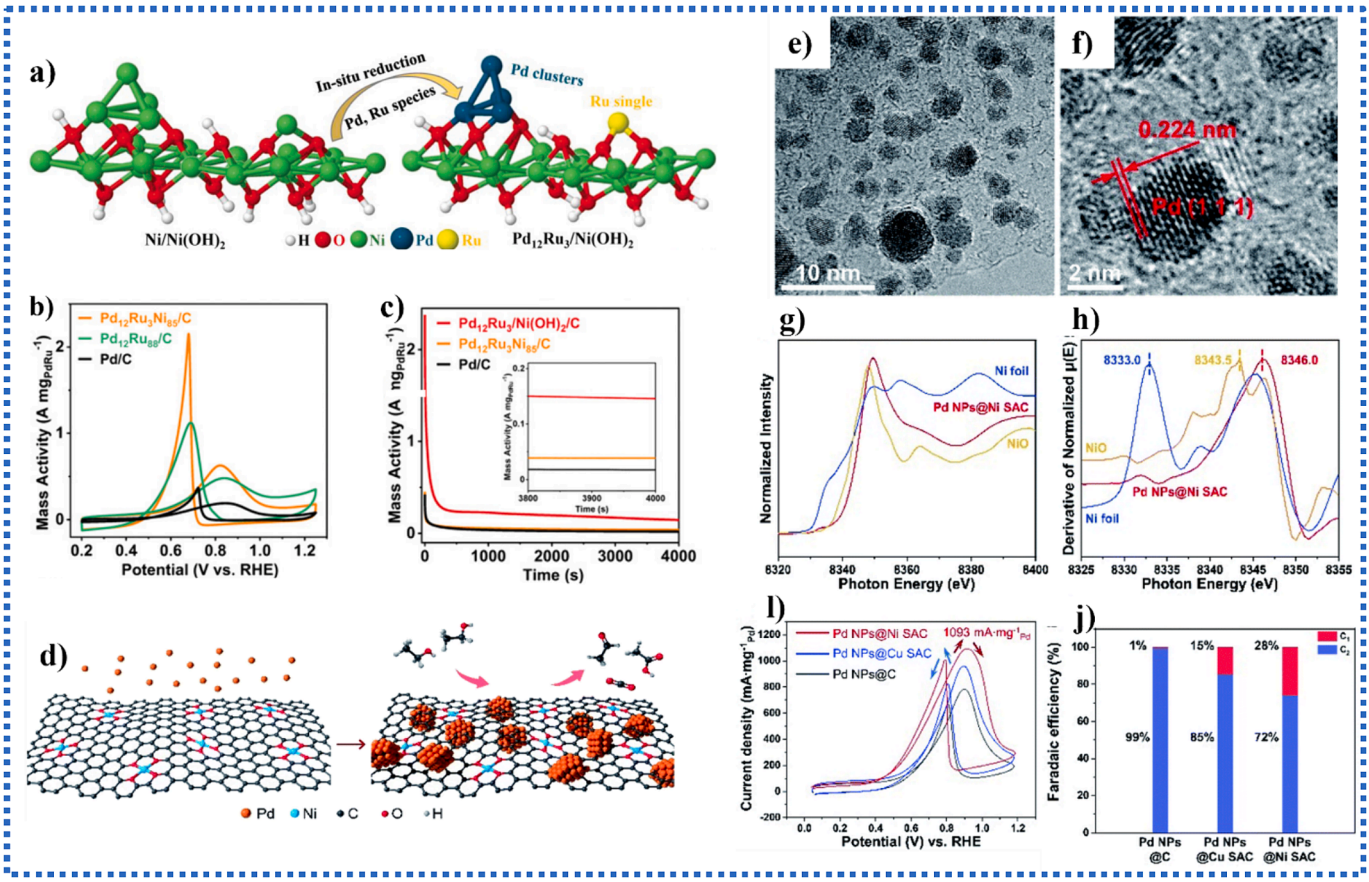


Fig. 6. a) Schematic illustrating the synthesis of $Pd_{12}Ru_3/Ni(OH)_2/C$, **b)** CV, and **c)** Linear sweep profile showing the stability of $Pd_{12}Ru_3/Ni(OH)_2/C$, and other electrocatalysts in 1 M KOH/1M EtOH. Reproduced from Ref. [54] with permission from Wiley-VCH, Copyright (2022). **d)** Schematic showing the synthesis procedure of Pd NPs@Ni SAC and the EOR process, **e)** and **f)** Pd NPs@Ni SAC TEM and HR-TEM micrographs, **g)** XANES spectra, **h)** first derivatives of the XANES region, **i)** CV curves of Pd NPs@Ni SAC, Pd NPs@Cu SAC and Pd NPs@C, and **j)** Faradaic efficiencies of C1 and *C*2 products. Reproduced from Ref. [100] with permission from RSC, Copyright (2022),

alloys (SAA). Besides the merit of improved stability, SAAs boost advantages such as easy scalability of synthesis routes and availability of more active sites which is beneficial for efficacy enhancement of electrocatalytic systems [102]. In view of this, Wang and co-workers [56] described ionic liquid (IL)-functionalized PdBi SAA aerogels formed by dispersing Bi single atoms on Pd nanowires ($IL/Pd_{50}Bi_1$) *via* $NaBH_4$ reduction, as illustrated in Fig. 7e, for the electrocatalysis of EOR. The metallic states of Bi L3-edge XANES spectra of $IL/Pd_{50}Bi_1$ and Bi powder were found to be similar (Fig. 7f) while EXAFs indicated the existence of Bi-Pd and Bi-O bonds (Fig. 7g). Electrochemical studies showed that E_{onset}, MA, and stability for the SAA were superior for $IL/Pd_{50}Bi_1$ than IL/Pd and commercial Pd/C. CO tests further indicated high tolerance towards poisoning by reaction intermediates, with the CO oxidation reaction occurring at lower potentials for the $IL/Pd_{50}Bi_1$ electrocatalyst. DFT calculations revealed that the Bi single atoms reduced the energy barrier of the rate-determining step, thus causing a facile EOR process and high electrocatalytic activity as indicated in Fig. 7h. The authors concluded that both the Bi single atoms and IL contributed to the electronic modulation effect and that the 3D aerogels backbone offered more access to the active sites resulting in enhanced mass transport and electron transfer and this high EOR efficiency for the $IL/Pd_{50}Bi_1$ material. Table 2 summarizes the efficient SAC electrocatalysts reported so far together with their synthesis methods, properties, and EOR electrochemistry in alkaline media.

5. Emerging supports

Improving the stability of the catalyst holds equal significance in achieving sustained, uninterrupted power output in ADAFCs. It is observed that the anodic catalysts degrade over prolonged operations due to various factors. Notably, the aggregation and detachment of Pd nanoparticles from the catalyst support, along with the corrosion of carbon support, are primary causes of catalyst degradation. Both issues predominantly hinge on the oxidation stability of the catalyst support. Hence, it is imperative to investigate stable catalyst supports that facilitate rapid charge transfer during the fuel oxidation process. The catalyst support serves several crucial functions, and any material considered for this role must meet specific desirable criteria, such as high specific surface area, enhanced electronic conductivity, suitable porosity, and strong-metal–metal interaction [103]. Vulcan carbon (XC-72R) is the most prevalent carbon substrate utilized for anchoring Pd-based EOR electrocatalysts, although its susceptibility to carbon corrosion is widely recognized owing to its hydrophilic properties, diminished graphitization content, and improved surface defect density [104,105]. Alternative materials like carbon nanotubes, graphene, carbon nanofibers, and graphitized carbon have been utilized to augment the longevity of Pd-based electrocatalysts [106,107]. These carbonaceous substrates offer superior characteristics compared to conventional Vulcan carbon, such as improved electronic conductivity, enhanced metal-support interaction, and better graphitic structure, all of which are crucial for retarding the kinetics of carbon corrosion [108,109].

5.1. Newly developed carbon supports

A study by Zhao *et al.* [19], outlined that despite the advancements in making durable carbon supports and strategies to mitigate carbon

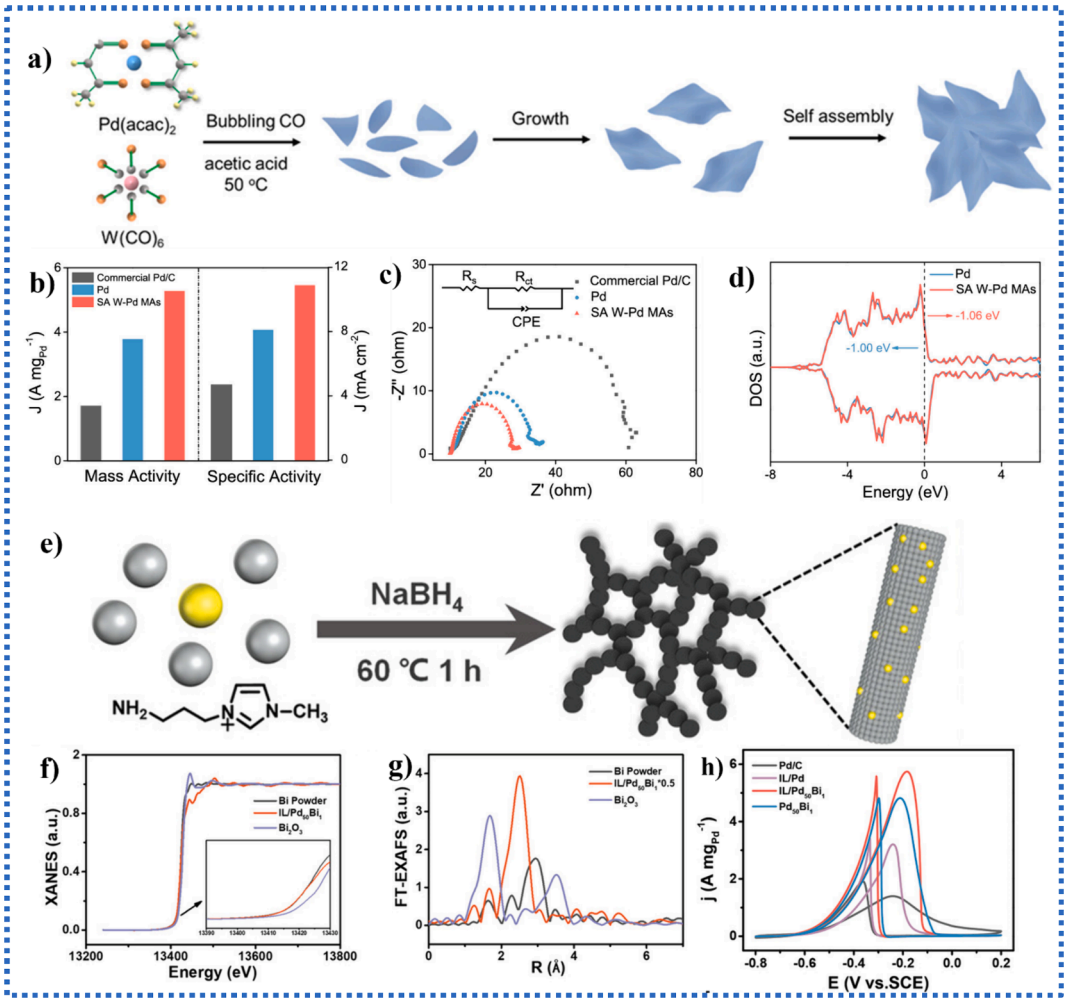


Fig. 7. **a)** Scheme showing the proposed model for a bubbling CO-induced gelation method for SA W-Pd MAs synthesis, **b)** MA and SA for EOR at peak potentials and **c)** EIS for SA W-Pd MAs, Pd and commercial Pd/C, **d)** PDOS plot of the Pd d-band for Pd and SA W-Pd. Reproduced from Ref. [101], with permission from ACS NANO, Copyright (2022). **e)** Schematic illustration of the synthesis of IL/$Pd_{50}Bi_1$ hydrogels, **f)** XANES spectra at Bi L3 edge and **g)** k3-weighted χ(k) function of the EXAFS spectra of Bi powder, Bi_2O_3, and IL/$Pd_{50}Bi_1$ aerogels, **h)** CV curves of IL/Pd, IL/$Pd_{50}Bi_1$, and $Pd_{50}Bi_1$ aerogels and commercial Pd/C catalysts in N_2-purged 1.0 M KOH/1M EtOH at 50 mVs^{-1}. Reprinted from Ref. [56], with permission from Wiley-VCH, Copyright (2021).

corrosion, support corrosion remains an unavoidable aspect during prolonged fuel cell operations. Consequently, logical progression demands the pursuit of highly stable carbon supports or the exploration of support materials with minimal carbon content or entirely devoid of carbon. Such endeavors are essential for achieving an exceptionally stable catalyst while maintaining optimal electrocatalytic activity levels.

Recently, Alfonso and co-workers [110] reported on an interesting carbon material derived from corncob, an agricultural waste product from corn, referred to as biochar. This corncob biochar was obtained by pyrolysis of corncob powder at 900℃ under N_2 and subsequently used as a Pd support to form Pd/CB900 for EOR electrocatalysis. Physicochemical characterization revealed more surface roughness and irregular porosity (see Fig. 8a) than conventional Vulcan carbon. The novel support also possessed oxygen functional groups which served as sites for Pd adsorption. According to XRD analysis, Pd/CB900 possessed smaller crystallite sizes than Pd/C, i.e. 3.26 nm and 7.28 nm, respectively, owing to the nature and the textural properties as well as the dispersion and favorable interaction between Pd the biochar support. Consequently, the Pd/CB900 material exhibited enhanced EOR activity (ECSA~31.51 m^2g^{-1}, Tafel slope = 297.6 ($mVdec^{-1}$), E_{onset} ~ 0.587 V, MA~20.77 $mAcm^{-2}$) than Pd/C (ECSA~22.56 m^2g^{-1}, Tafel slope = 309.27 $mVdec^{-1}$, E_{onset} ~ 0.537 V, MA~17.59 $mAcm^{-2}$). Our research group reported on the use of a carbon hybrid material derived from nanodiamond pyrolysis [111], as a support for EOR. This new carbon material consists of distinct multi-layer concentric architecture and is thus referred to as onion-like carbon (OLC). In this work, CeO_2 was incorporated into the OLC support through a sol–gel process, culminating in the synthesis of CeO_2/OLC. Subsequently, Pd was impregnated onto the CeO_2/OLC composite, yielding Pd-CeO_2/OLC nanostructures (see Fig. 8b). Experimental and theoretical investigations showed that, unlike carbon black, OLC had a strong influence on the alteration of the electronic states of Pd-CeO_2, resulting in improved EOR performance for the Pd-CeO_2/OLC electrocatalyst. As a result of the synergic contribution of OLC and CeO_2, the Pd-CeO_2/OLC electrocatalyst exhibited a superb power density of 27.15 $mWcm^{-2}$ (Fig. 8c) with remarkable stability (Fig. 8d) after 48 h on a membrane-free 3D-printed ADEFC, with power density 1.38, and 7.58-times higher that of Pd/OLC (19.72 mW cm^{-2}).

5.2. *Mxenes as a fascinating support material for EOR*

Mxenes have emerged as a possible non-carbon support for the deposition of Pd and Pd-based electrocatalysts for EOR. Mxenes are a class of 2D transition metal nitrides, carbides, carbon-nitrides with layers of $M_{n+1}X_nT_n$, where M represents a transitional metal (e.g., Sc, Ti, Zr, Hf, V, Nb, Ta, Cr, or Mo), "A" is an element from groups III–VI in the

Table 2
Pd-based SACs electrocatalysts for ethanol oxidation in alkaline environments.

SAC electrocatalyst	Synthesis method	Observed properties	Electrochemistry	Refs.
$Pd_{12}Ru_3/Ni(OH)_2/C$	Galvanic replacement method	Multiple active sites: Pd nanoclusters, Ru as single atoms, and $Ni(OH)_2$ as defective sites.	MA of 3.724 A mg_{PtPd}^{-1}, 20.9 % selectivity for C1 pathway	[54]
Pd NPs@Ni	Two-step method; freeze-drying and thermal annealing.	Graphene-line carbon sheets, Pd NPs sized between 2 to 5 nm, Ni as single atoms.	MA of 1093 mA mg_{Pd}^{-1}; 28 % selectivity for C1 pathway; 90 % MA retention after 4000 CVs, 50 % MA retention after 17 000 s CA.	[100]
SA W-Pd MAs	Bubbling CO-induced gelation in acetic acid at 50 °C	Abundant active sites, hierarchical nanoporous and W single atom-doped metallene Pd structure, average diameter of 1.21 nm, 2D microstructure	MA of 5.29 A $mg_{Pd}^{-}1$, SA of 10.9 mA cm^{-2}, 25.8 % selectivity for C1 pathway higher MA retention after 5000 s CA	[101]
$IL/Pd_{50}Bi_1$	One-step $NaBH_4$ reduction method	Accessible active sites, Bi as single atoms, 3D architectures of interconnected porous and extended nanowires with an average diameter of 5.1 nm.	Earlier E_{onset};1.6- and 4.1-times higher MA than IL/Pd and Pd/C; higher MA retained after 1 h CA	[56]

periodic table (such as Al, Ga, In, Tl, Si, Ge, Sn, Pb, P, As, Bi, S, or Te), and "X" is carbon and/or nitrogen and T represents chemical functional groups on the surface such as –OH, −O, −F and −Cl and n can be three integers 1, 2, 3, with $n + 1$ layers of transition metals sandwiching the n layers of carbon/or nitrogen or their mixtures [103,112,113]. Typically, Mxenes are generated by selectively etching using HF, to remove the "A" elements from $M_{n+1}AX_n$ phases, (see Fig. 9a). This process naturally generates –OH, −O, or −F groups at the terminations, resulting in MXenes with the formula $M_{n+1}X_nT_n$. These terminations are believed to play crucial roles such as enhancing hydrophilicity and controlling the electrical structure of MXenes thereby enabling the application of the materials in energy conversion and energy storage [112]. More importantly, these terminations facilitate the adsorption of metal precursors by electrostatic interactions, thus allowing the anchoring of metal nanoparticles [114].

The exploration of MXenes as supports for EOR electrocatalysts may have been inspired by previous studies on TiC and TiN-based nanoparticles which have been deployed as corrosion-resistant supports for Pt and its alloys for oxygen reduction reaction (ORR) and methanol oxidation (MOR) [115,116]. Given that MXenes resemble TiC and TiN-based nanoparticles, where Ti and C were observed to confer respective corrosion resistance and electrical conductivity for ORR and MOR, it is widely believed that these properties can be extended to Ti-based MXenes. Moreover, Ti-MXenes possess a large surface area conducive for the deposition of metal nanoparticles, while the surface functional groups (such as –OH and −F) impart well-balanced hydrophilicity and hydrophobicity. Additionally, the −F termination endows stability in harsh electrolytes, resisting carbon corrosion and catalyst aggregation, dissolution, and Ostwald ripening, as opposed to the traditional Vulcan carbon catalyst support [103,109]. On the other hand, 2D $Ti_3C_2T_x$ has been reported to effectively alter the electronic structure of deposited metal nanoparticles for enhanced electrocatalytic activity and CO poisoning resistance. Recent theoretic simulations and experimental findings have also indicated robust strong metal-support interactions (SMSI) between 2D MXenes and deposited nanoparticles, a feat that endows enhanced stability [117,118].

Peng and co-workers [114] supported ultrathin layers of Pd metallenes on $Ti_3C_2T_x$ MXene (Pdene/$Ti_3C_2T_x$) *via* in-situ growth under mild conditions. Due to the strong SMSI, the Pdene/$Ti_3C_2T_x$ electrocatalyst, after optimization, exhibited an exceptional MA of 7.47 A $mg_{Pd}{}^{-1}$ in 1 M KOH, high CO tolerance resulting in excellent stability and high selectivity for C1 pathway. After *in-situ* attenuated total reflection-infrared (ATR-IR) spectroscopy studies and DFT calculations, the authors attributed the excellent EOR performance to strong Pd-OH bonds which facilitated oxidative removal of toxic CO intermediates and that the Pd metallenes stabilized on the $Ti_3C_2T_x$ support reduced the energy barrier of $*CH_3CO$ intermediates. The interaction between supports and loaded Pd atoms can be further improved by doping MXenes with heteroatoms. The doping effect modifies the electronic structure of MXene support even further for a stronger SMSI, preventing agglomeration, and enhances the EOR electrocatalytic activity. Chen *et al* [119] reported an *N*-doped Ti_3C_2 supported Pd-based electrocatalyst for application as an anode material for EOR. After optimizing HF etching times (i.e. 28 hrs selected as the most suitable time), the authors used NH_3H_2O as an *N* dopant to form Pd/*N*-Ti_3C_2-28 h, which exhibited higher Pd content (at the same loading) than the non-doped Pd/ Ti_3C_2-28 h material. This suggests that the doping effect facilitated a better Pd dispersion, resulting in a high ECSA and ultimately a better EOR efficiency than the non-doped material and commercial Pd/C. In the same vein, the same group [120] outlined another study where they co-doped Ti_3C_2 with B and N using dimethylamine borane (DB) as a co-doping precursor and a Pd reducing agent for making a Pd/DB–Ti_3C_2 through a one-step method for application in EOR as indicated in Fig. 9b. The co-doping process resulted in the electronic modulation of Pd electrons in Pd/DB-Ti_3C_2 marked by a lower *d*-band center which was far from the Fermi energy. This effect broadened the D bandwidth and caused a negative shift in the *d*-band center, resulting in poor adsorption of the reaction intermediates on the catalyst surface, thus improving the EOR electrocatalysis. To this effect, the catalyst showed excellent durability of 91.1 % MA after 2000 s CV cycles, far better than that of commercial Pd/C. Li and co-workers [121] reported an interesting study where $Ti_3C_2T_x$ nanosheets were utilized as a 'spacer' to prevent the agglomeration of graphene. Graphene tends to agglomerate irreversibly due to strong π-π interactions, van der Walls forces, and hydrophobic interactions, ultimately leading to the significant reduction of its specific surface area and porosity. The authors used a hydrothermal, and Pd salt reduction method to intercalate $Ti_3C_2T_x$ into nitrogen-doped-graphene (NG) and subsequently immobilized Pd to obtain Pd/$Ti_3C_2T_x$@-NG. The resultant highly porous and large surface area (confirmed by Brunauer-Emmett-Teller) Pd/$Ti_3C_2T_x$@-NG exhibited high activity and high stability, retaining ~ 31.4 % MA after 500 CV cycles, far better than Pd/NG (18.8 %) and commercial Pd/C (8.6 %). The authors attributed the high performance of the electrocatalyst to the intercalated, highly conductive $Ti_3C_2T_x$ which opened more pores and channels for enhanced mass transport charge transport, respectively, resulting in more exposed growth sites for embedding Pd nanocrystals. Peng *et al.* [35] unveiled an interesting strategy of using sulfur stabilization to combat sintering associated with HEA nanoparticle synthesis at extremely high temperatures. HEAs are usually produced *via* carbothermal shock (~2000 K), fast-moving bed pyrolysis (~923 K), microwave heating (~1850 K), etc, which may lead to thermal sintering, unavoidably resulting in significantly reduced specific surface area and a steep decrease in catalyst activity. The authors introduced sulfur stabilization where S-modified MXene (S−$Ti_3C_2T_x$) supported a PtPdCuNiCo HEA by forming strong metal-sulfur bonds. This resulted in significantly increased interfacial adhesion strength, hence greatly suppressing HEA nanoparticle sintering by impeding both particle migration and metal atom diffusion. The resultant quinary PtPdCuNiCo HEA-S-$Ti_3C_2T_x$ exhibited ultra-high MA 7.03 A

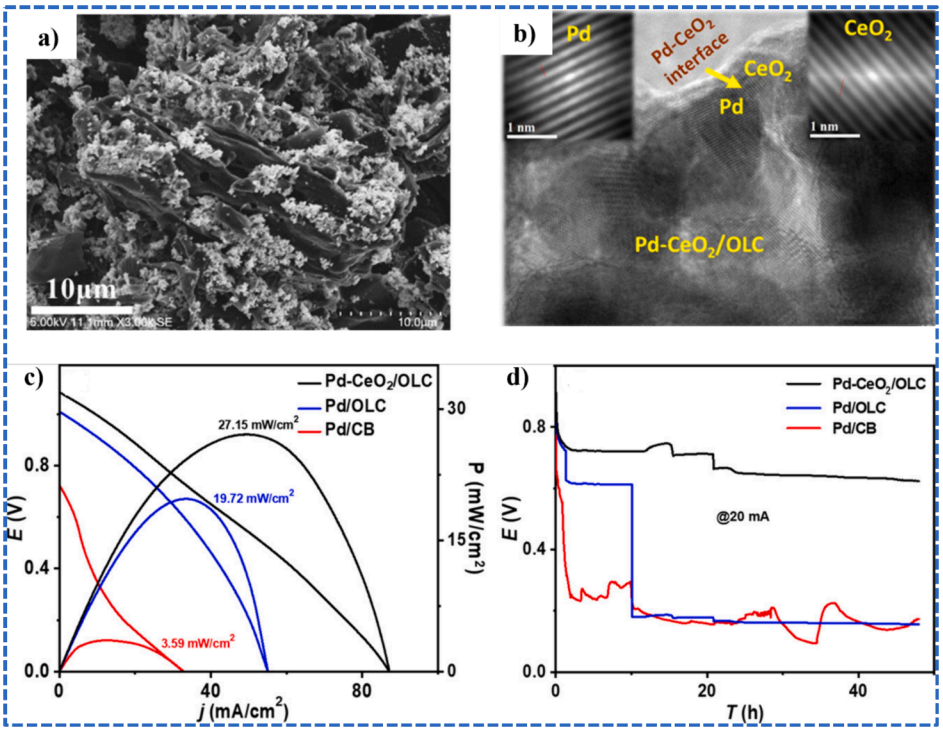


Fig. 8. **a)** SEM micrograph of Pd/CB900. Reprinted from Ref. [110], with permission from The Chemical Society Located in Taipei & Wiley-VCH GmbH, Copyright (2024), **b)** High-magnification TEM images of Pd, CeO_2 and Pd-CeO_2/OLC and FFT transforms of Pd and CeO_2, **c)** Voltage-power curves, galvanostatic discharge stability test of the Pd-CeO_2/OLC and other electrocatalysts in 2.0 M EtOH/2.0 M KOH solutions. Ref. Adapted from [111].

mg^{-1}_{Pt+Pd}, which was respectively 5.17 and 4.34 times higher than those of the commercial Pd/C and Pt/C catalysts. The catalyst also showed remarkable stability, retaining 93 % MA after 500 accelerated cycles, thanks to the strong SMSI. Table 3 summarizes the features of emerging carbon materials and MXenes as support materials for EOR.

6. Challenges, outlook, perspectives, and concluding remarks

ADEFCs have emerged as a promising alternate energy source. However, Faradaic efficiency is a critical problem specific to ethanol oxidation since it is unlikely to undergo the C1 pathway leading to reduced fuel utilization efficiency and low Faradaic efficiency (typically < 30 %) [30]. Research attempts to cleave the C—C bond are still ongoing. This article reviews recent advances in emerging EOR electrocatalysts, particularly Pd-based HEMs and SACs, and summarizes their electrocatalytic properties for EOR. New developments in catalytic supports are also discussed with special emphasis on newly developed carbons and MXenes. HEMs boast of quadruple effects namely entropy, lattice distortion, sluggish diffusion, and cocktail effects, endowing unique catalytic properties capable of improving EOR. These materials provide diverse surface metal sites with highly tunable adsorption energies for reaction intermediates. For example, the ample active sites of PGM-HEA efficiently catalyzed the C—C bond cleavage for EOR catalysis *via* the 12 electron/12 proton process. On the other hand, NHEA@NHEA-Pd exhibited the highest activity retention of 98.8 % after 2000 CVs. However, PtPdFeCoNiSnMn HEA (Pt/Pd HEA) represents the highest performing Pd HEM electrocatalysts for EOR today with approximately 100 % Faradaic efficiency for C—C cleavage, and 99.99 % and 99.97 % current density retention after and 30 000 and 50 000, respectively. Its assembled ADEFC demonstrated a power density of 0.72 Wcm^{-2} with a durable operation for 1200 h (50 days). This clearly shows that HEMs are capable of defeating the sluggish EOR process. Despite SACs having highly exposed active sites, one of their observed limitation is the low C1 selectivity. The highest C1 selectivity reported for a SAC to date was that reported for the Pd NPs@Ni SAC electrocatalyst, at only 28 %. The same SAC electrocatalyst retained a mere 50 % MA after 17 000 s CA. This may suggest that the single-site feature may limit the application of SACs in catalytic processes where cascade reactions are involved, and where multimetal active sites are maybe suitable. However, a study showing the synergies of SACs and HEMs for EOR has not been reported to date, which means that this is a route that is yet to be explored. To fully understand how active sites, elemental distribution and defect impact EOR catalytic properties, it is necessary to incorporate advanced characterisation tools such as machine learning-assisted data acquisition to capture critical dynamic changes in HEMs during the EOR electrocatalytic process. Moreover, information such as lattice strain, surface atomic structure, chemical diffusion, and electronic structure of HEMs may also be obtained, providing more input for theoretical calculations and insights into the reaction pathways. This can allow ML to significantly aid in the design and optimization of electrocatalysts i.e. HEMs and SACs for ethanol oxidation reaction. Thus, by accurately predicting the properties and behaviors of these materials, ML can streamline the discovery and development of superior electrocatalysts [125,126].

Due to poor electrical conductivity, MXenes (~1.2×10^{-1} Scm^{-1}) may need to be doped with heteroatoms (e.g. N, S, etc) for them to compete with Vulcan carbon (3.4×10^{-1} Scm^{-1}) for EOR electrocatalysis [127,128].. On another note, Vizza's laboratory demonstrated that it is possible to improve the stability of EOR electrocatalysts by combining Vulcan carbon supports with CeO_2 which can facilitate the oxidation of Pd^0 to Pd - OH_{ads} for improved EOR [6]. Thus, Pd-based HEMs can be stabilized on Vulcan carbon-CeO_2 to form Pd-based HEMs/C-CeO_2. For instance, our laboratory is exploring the utility of Pd-based HEMs such as Pd-HESOx/C-CeO_2 for the electrocatalysis of EOR.

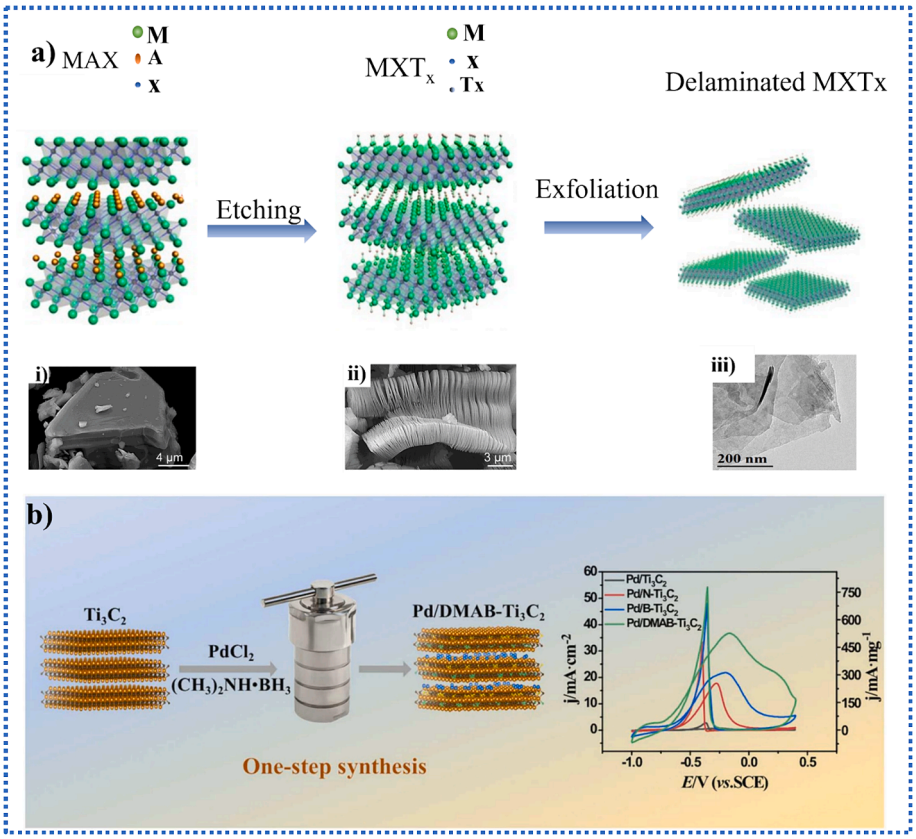


Fig. 9. a) Shows the synthesis of MXenes from a precursor MAX phase by etching using HF. Some layers are removed and replaced by surface terminals T_x such as −O, –OH, and/or −F to form multilayered MXenes. Exfoliation of multilayered MXene into 2D flakes becomes possible through sonication or intercalation of cations and organic molecules. (i) SEM micrographs of bulk Mo_2CT_x flake, (ii) SEM micrograph of $Ti_3C_2T_x$ after etching, (iii) TEM image of $Ti_3C_2T_x$ flake after exfoliation. Image (i) and (7ii) adapted from Ref. [122], with permission from ACS Nano, Copyright (2012). TEM image (iii) of isolated $Ti_3C_2T_x$ adapted from Ref. [123], with permission from Elsevier Copyright (2019). **B)** One-step hydrothermal procedure for co-doping and reducing Pd to make Pd/DMAB-Ti_3C_2. Reprinted from Ref. [124], with permission from Elsevier. Copyright (2023).

Table 3
Emerging carbon and MXene support materials for Pd-based electrocatalysts for EOR.

Support type	Support name	Preparation method	Properties	Electrocatalyst durability	Refs.
Carbons	CB900	Pyrolysis of corncob biochar powder at 900°C under H_2.	Oxygen functional groups on the surface enhance the adsorption of Pd.	50.64 ± 2.99 % geometric activity after 3000 s CA	[110]
	Onion-like carbon	Pyrolysis of high purity nanodiamond at 1300°C under H_2	Nature of the carbon material exerted a strong influence on the electronic states of Pd-CeO_2	~78 % voltage retention during a 48-hour discharge	[111]
MXenes	$Ti_3C_2T_x$	*in-situ* growth under mild conditions	Pd atoms embedded in Ti vacancies. Pd forms strong Pd-C bonds with C atoms.	74 % MA retention after 500 CVs	[114]
	N-Ti_3C_2	One-step hydrothermal method using NH_3-H_2O as *N* source	*N* doping provided high Pd dispersion.	78.3 % MA retention after 200 CVs	[119]
	DB–Ti_3C_2	B, N co-oping with DB as the precursor *via* hydrothermal reaction	B-doped MXene provided a highly efficient support for Pd.	91.1 % MA retention after 2000 CVs	[120]
	$Ti_3C_2T_x$@-NG	Simple hydrothermal procedure	Spacer for graphene to prevent its agglomeration.	~31.4 % MA retention after 500 CVs	[121]
	S−$Ti_3C_2T_x$	Freeze-drying	Support for PtPdCuNiCo HEA *via* the formation of strong metal-S bonds. Prevents HEA sintering.	93 % MA retention after 500 CVs	[35]

CRediT authorship contribution statement

Colani Fakude: Writing – review & editing. **Aderemi Haruna:** Writing – review & editing. **Kenneth I. Ozoemena:** Conceptualization, Supervision, Writing – review & editing.

Declaration of competing interest

The authors declare that they have no known competing financial interests or personal relationships that could have appeared to influence the work reported in this paper.

Data availability

Data will be made available on request.

Acknowledgments

The authors are grateful for the support of the NRF (South Africa)/ FWO (Belgium) Joint Science and Technology Research Collaboration for the Project "Electrochemistry, nanostructured electrocatalysts for tackling substance abuse, and the DSI-NRF-Wits SARChI Chair in Materials Electrochemistry and Energy Technologies (MEET) (UID No.: 132739). C.F. appreciates the financial support from the Wits prestigious Phillip Vallentine Tobias Educational Bursary for his PhD studies, and the NRF for PhD scholarship.

References

[1] D.N. Gemechu, A.M. Mohammed, M. Redi, D. Bessarabov, Y.S. Mekonnen, K. O. Obodo, First principles-based approaches for catalytic activity on the dehydrogenation of liquid organic hydrogen carriers: a review, Int. J. Hydrogen Energy 48 (2023) 33186–33206.

[2] C.V. Almeida, F. Colmati, E.G. Ciapina, K.I. Eguiluz, G.R. Salazar-Banda, Nanowires of Pd and Pd alloys for fuel cell applications: a review of the current state-of-the-art, J. Electroanal. Chem. 955 (2024) 118073.

[3] L. Yaqoob, T. Noor, N. Iqbal, A comprehensive and critical review of the recent progress in electrocatalysts for the ethanol oxidation reaction, RSC Adv. 11 (2021) 16768–16804.

[4] A. K. Ipadeola, N. Z. Lisa Mathebula, M. V. Pagliaro, H. A. Miller, F. Vizza, V. Davies, Q. Jia, F. Marken, and K. I. Ozoemena, "Unmasking the Latent Passivating Roles of Ni(OH)2 on the Performance of Pd–Ni Electrocatalysts for Alkaline Ethanol Fuel Cells," *ACS Applied Energy Materials,* 3 (2020) 8786-8802.

[5] H.A. Miller, A. Lavacchi, F. Vizza, M. Marelli, F. Di Benedetto, F. D'Acapito, Y. Paska, M. Page, D.R. Dekel, A Pd/C-CeO2 anode catalyst for high-performance platinum-free anion exchange membrane fuel cells, Angew. Chem. Int. Ed. 55 (2016) 6004–6007.

[6] V. Bambagioni, C. Bianchini, Y. Chen, J. Filippi, P. Fornasiero, M. Innocenti, A. Lavacchi, A. Marchionni, W. Oberhauser, F. Vizza, Energy efficiency enhancement of ethanol electrooxidation on pd–ceo2/c in passive and active polymer electrolyte-membrane fuel cells, ChemSusChem 5 (2012) 1266–1273.

[7] K.I. Ozoemena, Nanostructured platinum-free electrocatalysts in alkaline direct alcohol fuel cells: catalyst design, principles and applications, RSC Adv. 6 (2016) 89523–89550.

[8] M. Liu, F. Yu, C. Ma, X. Xue, H. Fu, H. Yuan, S. Yang, G. Wang, X. Guo, L. Zhang, Effective oxygen reduction reaction performance of FeCo alloys in situ anchored on nitrogen-doped carbon by the microwave-assistant carbon bath method and subsequent plasma etching, Nanomaterials 9 (2019) 1284.

[9] H. Fang, T. Huang, Y. Sun, B. Kang, D. Liang, S. Yao, J. Yu, M.M. Dinesh, S. Wu, J. Y. Lee, Metal-organic framework-derived core-shell-structured nitrogen-doped CoCx/FeCo@ C hybrid supported by reduced graphene oxide sheets as high performance bifunctional electrocatalysts for ORR and OER, J. Catal. 371 (2019) 185–195.

[10] Q. Liu, S. Cao, Y. Qiu, Effect of carbonization temperature on bimetallic FeCo-N/C nanofiber electrocatalysts for oxygen reduction reaction in sulfuric acid solution, Int. J. Hydrogen Energy 42 (2017) 29274–29282.

[11] Z. Liu, Z. Zhao, B. Peng, X. Duan, Y. Huang, Beyond extended surfaces: understanding the oxygen reduction reaction on nanocatalysts, J. Am. Chem. Soc. 142 (2020) 17812–17827.

[12] Y. Wang, L. Li, L. Hu, L. Zhuang, J. Lu, B. Xu, A feasibility analysis for alkaline membrane direct methanol fuel cell: thermodynamic disadvantages versus kinetic advantages, Electrochem. Commun. 5 (2003) 662–666.

[13] M. Cifrain, K. Kordesch, Advances, aging mechanism and lifetime in AFCs with circulating electrolytes, J. Power Sources 127 (2004) 234–242.

[14] T. Ramulifho, K.I. Ozoemena, R.M. Modibedi, C.J. Jafta, M.K. Mathe, Electrocatalytic oxidation of ethylene glycol at palladium-bimetallic nanocatalysts (PdSn and PdNi) supported on sulfonate-functionalised multi-walled carbon nanotubes, J. Electroanal. Chem. 692 (2013) 26–30.

[15] W. Du, K.E. Mackenzie, D.F. Milano, N.A. Deskins, D. Su, X. Teng, Palladium–Tin alloyed catalysts for the ethanol oxidation reaction in an alkaline medium, ACS Catal. 2 (2012) 287–297.

[16] J. Chang, G. Wang, C. Li, Y. He, Y. Zhu, W. Zhang, M. Sajid, A. Kara, M. Gu, Y. Yang, Rational design of septenary high-entropy alloy for direct ethanol fuel cells, Joule 7 (2023) 587–602.

[17] K. Vasić, Ž. Knez, M. Leitgeb, Bioethanol production by enzymatic hydrolysis from different lignocellulosic sources, Molecules 26 (2021) 753.

[18] A. Susmozas, R. Martín-Sampedro, D. Ibarra, M.E. Eugenio, R. Iglesias, P. Manzanares, A.D. Moreno, Process strategies for the transition of 1G to advanced bioethanol production, Processes 8 (2020) 1310.

[19] S. Jadali, M.A. Kamyabi, J. Solla-Gullón, E. Herrero, Effect of pd on the electrocatalytic activity of pt towards oxidation of ethanol in alkaline solutions, Appl. Sci. 11 (2021) 1315.

[20] S. Mohanapriya, D. Gopi, Electro-oxidation of alcohols-Recent advancements in synthesis and applications of palladium core-shell nanostructured model catalysts, Renew. Sustain. Energy Rev. 148 (2021) 111211.

[21] A.M. Damjanović, B. Koyutürk, Y.-S. Li, D. Menga, C. Eickes, H.A. El-Sayed, H. A. Gasteiger, T.-P. Fellinger, M. Piana, Loading Impact of a PGM-free catalyst on the mass activity in proton exchange membrane fuel cells, J. Electrochem. Soc. 168 (2021) 114518.

[22] S. Guo, S. Zhang, X. Sun, S. Sun, Synthesis of ultrathin FePtPd nanowires and their use as catalysts for methanol oxidation reaction, J. Am. Chem. Soc. 133 (2011) 15354–15357.

[23] I. Kim, O.H. Han, S.A. Chae, Y. Paik, S.H. Kwon, K.S. Lee, Y.E. Sung, H. Kim, Catalytic reactions in direct ethanol fuel cells, Angew. Chem. Int. Ed. 50 (2011) 2270–2274.

[24] S.C. Lai, M.T. Koper, Electro-oxidation of ethanol and acetaldehyde on platinum single-crystal electrodes, Faraday Discuss. 140 (2009) 399–416.

[25] G. Cui, S. Song, P.K. Shen, A. Kowal, C. Bianchini, First-principles considerations on catalytic activity of Pd toward ethanol oxidation, J. Phys. Chem. C 113 (2009) 15639–15642.

[26] T. Matthews, S.P. Mbokazi, T.H. Dolla, S.S. Gwebu, K. Mugadza, K. Raseruthe, L. L. Sikeyi, K.A. Adegoke, O.D. Saliu, A.S. Adekunle, Electrocatalyst Performances in direct alcohol fuel cells: defect engineering protocols, electrocatalytic pathways, key parameters for improvement, and breakthroughs on the horizon, Small Sci. 2300057 (2023).

[27] Y.-Y. Yang, J. Ren, Q.-X. Li, Z.-Y. Zhou, S.-G. Sun, W.-B. Cai, Electrocatalysis of ethanol on a Pd electrode in alkaline media: an in situ attenuated total reflection surface-enhanced infrared absorption spectroscopy study, ACS Catal. 4 (2014) 798–803.

[28] C. Zhu, B. Lan, R.-L. Wei, C.-N. Wang, Y.-Y. Yang, Potential-dependent selectivity of ethanol complete oxidation on Rh electrode in alkaline media: a synergistic study of electrochemical ATR-SEIRAS and IRAS, ACS Catal. 9 (2019) 4046–4053.

[29] R. B. Kutz, B. r. Braunschweig, P. Mukherjee, D. D. Dlott, and A. Wieckowski, "Study of ethanol electrooxidation in alkaline electrolytes with isotope labels and sum-frequency generation," *The Journal of Physical Chemistry Letters,* 2 (2011) 2236-2240.

[30] X. Fu, C. Wan, Y. Huang, X. Duan, Noble metal based electrocatalysts for alcohol oxidation reactions in alkaline media, Adv. Funct. Mater. 32 (2022) 2106401.

[31] Z. Liang, T. Zhao, J. Xu, L. Zhu, Mechanism study of the ethanol oxidation reaction on palladium in alkaline media, Electrochim. Acta 54 (2009) 2203–2208.

[32] L. Wang, V. Bambagioni, M. Bevilacqua, C. Bianchini, J. Filippi, A. Lavacchi, A. Marchionni, F. Vizza, X. Fang, P.K. Shen, Sodium borohydride as an additive to enhance the performance of direct ethanol fuel cells, J. Power Sources 195 (2010) 8036–8043.

[33] T. Li, Q. Wang, W. Zhang, H. Li, Y. Wang, J. Liu, Length-tunable Pd(2)Sn@Pt core-shell nanorods for enhanced ethanol electrooxidation with concurrent hydrogen production, Chem Sci 14 (2023) 9488–9495.

[34] J. D. Lović, S. Eraković Pantović, L. Z. Rakočević, N. L. Ignjatović, S. B. Dimitrijević, and N. D. Nikolić, "A Novel Two-Step Electrochemical Deposition Method for Sn-Pd Electrocatalyst Synthesis for a Potential Application in Direct Ethanol Fuel Cells," *Processes,* 11 (2023) 120.

[35] W. Peng, Y.R. Lu, H. Lin, M. Peng, T.S. Chan, A. Pan, Y. Tan, Sulfur-Stabilizing Ultrafine High-Entropy Alloy Nanoparticles on MXene for Highly Efficient Ethanol Electrooxidation, ACS Nano 17 (2023) 22691–22700.

[36] C.L. Green, A. Kucernak, Determination of the platinum and ruthenium surface areas in platinum– ruthenium alloy electrocatalysts by underpotential deposition of copper. I. Unsupported catalysts, J. Phys. Chem. B 106 (2002) 1036–1047.

[37] T. Bligaard, J.K. Nørskov, Ligand effects in heterogeneous catalysis and electrochemistry, Electrochim. Acta 52 (2007) 5512–5516.

[38] M. Mavrikakis, B. Hammer, J.K. Nørskov, Effect of strain on the reactivity of metal surfaces, Phys. Rev. Lett. 81 (1998) 2819.

[39] Z. Quan, Y. Wang, J. Fang, High-index faceted noble metal nanocrystals, Acc. Chem. Res. 46 (2013) 191–202.

[40] D. Wu, K. Kusada, T. Yamamoto, T. Toriyama, S. Matsumura, S. Kawaguchi, Y. Kubota, H. Kitagawa, Platinum-group-metal high-entropy-alloy nanoparticles, J. Am. Chem. Soc. 142 (2020) 13833–13838.

[41] O.O. Fashedemi, K.I. Ozoemena, Comparative electrocatalytic oxidation of ethanol, ethylene glycol and glycerol in alkaline medium at Pd-decorated FeCo@ Fe/C core-shell nanocatalysts, Electrochim. Acta 128 (2014) 279–286.

[42] Z. Liu, X.Y. Ling, X. Su, J.Y. Lee, Carbon-supported Pt and PtRu nanoparticles as catalysts for a direct methanol fuel cell, J. Phys. Chem. B 108 (2004) 8234–8240.

[43] R. Mancharan, J.B. Goodenough, Methanol oxidation in acid on ordered NiTi, J. Mater. Chem. 2 (1992) 875–887.

[44] A.M. Hofstead-Duffy, D.-J. Chen, S.-G. Sun, Y.J. Tong, Origin of the current peak of negative scan in the cyclic voltammetry of methanol electro-oxidation on Pt-based electrocatalysts: a revisit to the current ratio criterion, J. Mater. Chem. 22 (2012) 5205–5208.

[45] X. Chen, C. Si, Y. Gao, J. Frenzel, J. Sun, G. Eggeler, Z. Zhang, Multi-component nanoporous platinum–ruthenium–copper–osmium–iridium alloy with enhanced electrocatalytic activity towards methanol oxidation and oxygen reduction, J. Power Sources 273 (2015) 324–332.

[46] W. Huang, X.Y. Ma, H. Wang, R. Feng, J. Zhou, P.N. Duchesne, P. Zhang, F. Chen, N. Han, F. Zhao, Promoting effect of Ni (OH) 2 on palladium nanocrystals leads to greatly improved operation durability for electrocatalytic ethanol oxidation in alkaline solution, Adv. Mater. 29 (2017) 1703057.

[47] J. De Souza, S. Queiroz, K. Bergamaski, E.R. Gonzalez, F.C. Nart, Electro-oxidation of ethanol on Pt, Rh, and PtRh electrodes. A study using DEMS and in-situ FTIR techniques, J. Phys. Chem. B 106 (2002) 9825–9830.

[48] Z. Liang, L. Song, S. Deng, Y. Zhu, E. Stavitski, R.R. Adzic, J. Chen, J.X. Wang, Direct 12-electron oxidation of ethanol on a ternary Au (core)-PtIr (shell) electrocatalyst, J. Am. Chem. Soc. 141 (2019) 9629–9636.

[49] M. Schalenbach, O. Kasian, M. Ledendecker, F.D. Speck, A.M. Mingers, K. J. Mayrhofer, S. Cherevko, The electrochemical dissolution of noble metals in alkaline media, Electrocatalysis 9 (2018) 153–161.

[50] Z. Wang, E. Tada, A. Nishikata, Communication—platinum dissolution in alkaline electrolytes, J. Electrochem. Soc. 163 (2016) C853.

[51] G. Zhao, C. Fang, J. Hu, D. Zhang, Platinum-based electrocatalysts for direct alcohol fuel cells: enhanced performances toward alcohol oxidation reactions, ChemPlusChem 86 (2021) 574–586.

[52] J. Hao, B. Liu, M. Takahashi, S. Maenosono, J. Yang, Large Au@ Pd/PdO x core–porous shell nanoparticles as efficient ethanol oxidation electrocatalysts, Cat. Sci. Technol. 13 (2023) 4141–4147.

[53] Z. Zhao, L. Zhang, X. Ma, Y. Min, Q. Xu, Q. Li, Pd3Pb1@ Pt2 core–shell concave nanocubes to boost the ethanol oxidation reaction, Electrochim. Acta 442 (2023) 141866.

[54] A. Pei, G. Li, L. Zhu, Z. Huang, J. Ye, Y.C. Chang, S.M. Osman, C.W. Pao, Q. Gao, B.H. Chen, Nickel hydroxide-supported Ru single atoms and Pd nanoclusters for enhanced electrocatalytic hydrogen evolution and ethanol oxidation, Adv. Funct. Mater. 32 (2022) 2208587.

[55] W. Zhou, L. Gao, Y. Zhang, T. Hu, Composites of Ni-MOF and polyaniline hydrogel for carbon monoxide resistant excellent catalysts of ethanol oxidation reaction, Int. J. Hydrogen Energy 46 (2021) 27128–27137.

[56] H. Wang, L. Jiao, L. Zheng, Q. Fang, Y. Qin, X. Luo, X. Wei, L. Hu, W. Gu, J. Wen, PdBi single-atom alloy aerogels for efficient ethanol oxidation, Adv. Funct. Mater. 31 (2021) 2103465.

[57] A.K. Ipadeola, R. Barik, S.C. Ray, K.I. Ozoemena, Bimetallic Pd/SnO2 Nanoparticles on Metal Organic Framework (MOF)-Derived Carbon as Electrocatalysts for Ethanol Oxidation, Electrocatalysis 10 (2019) 366–380.

[58] J. Wang, B. Zhang, W. Guo, L. Wang, J. Chen, H. Pan, W. Sun, Toward electrocatalytic methanol oxidation reaction: Longstanding debates and emerging catalysts, Adv. Mater. 2211099 (2023).

[59] T.D.S. Almeida, Y. Yu, A. De Andrade, H.D. Abruña, Employing iron and nickel to enhance ethanol oxidation of Pd-based anodes in alkaline medium, Electrochim. Acta 295 (2019) 751–758.

[60] L. Palma, T. Almeida, A. de Andrade, Comparative study of catalyst effect on ethanol electrooxidation in alkaline medium: Pt-and Pd-based catalysts containing Sn and Ru, J. Electroanal. Chem. 878 (2020) 114592.

[61] C. Liang, R. Zhao, T. Chen, Y. Luo, J. Hu, P. Qi, W. Ding, Recent Approaches for Cleaving the C— C Bond During Ethanol Electro-Oxidation Reaction, Adv. Sci. 2308958 (2024).

[62] H. Qiu, B. Yuan, C. Zhao, J. Dang, C. Zhang, Q. Wang, L. Xia, H. Miao, J. Yuan, A high-entropy and low-cobalt perovskite of La0. 7Sr0. 3Co0. 2Mn0. 2Ni0. 2Fe0. 2Al0. 2O3-x for both oxygen evolution and methanol oxidation reactions, Int. J. Hydrogen Energy 51 (2024) 593–604.

[63] H. Li, J. Lai, Z. Li, L. Wang, Multi-Sites Electrocatalysis in High-Entropy Alloys, Adv. Funct. Mater. 31 (2021) 2106715.

[64] Y. Ma, Y. Ma, Q. Wang, S. Schweidler, M. Botros, T. Fu, H. Hahn, T. Brezesinski, B. Breitung, High-entropy energy materials: challenges and new opportunities, Energ. Environ. Sci. 14 (2021) 2883–2905.

[65] T.A.A. Batchelor, J.K. Pedersen, S.H. Winther, I.E. Castelli, K.W. Jacobsen, J. Rossmeisl, High-Entropy Alloys as a Discovery Platform for Electrocatalysis, Joule 3 (2019) 834–845.

[66] H.-J. Qiu, G. Fang, Y. Wen, P. Liu, G. Xie, X. Liu, S. Sun, Nanoporous high-entropy alloys for highly stable and efficient catalysts, J. Mater. Chem. A 7 (2019) 6499–6506.

[67] Y. Sun, S. Dai, "High-entropy materials for catalysis: A new frontier, Sci. Adv. 7 (2021) eabg1600.

[68] J.-W. Yeh, Alloy design strategies and future trends in high-entropy alloys, JOM 65 (2013) 1759–1771.

[69] A.K. Ipadeola, A.K. Lebechi, L. Gaolatlhe, A.B. Haruna, M. Chitt, K. Eid, A. M. Abdullah, K.I. Ozoemena, Porous high-entropy alloys as efficient electrocatalysts for water-splitting reactions, Electrochem. Commun. 136 (2022) 107207.

[70] C.M. Rost, E. Sachet, T. Borman, A. Moballegh, E.C. Dickey, D. Hou, J.L. Jones, S. Curtarolo, J.-P. Maria, Entropy-stabilized oxides, Nat. Commun. 6 (2015) 8485.

[71] A. Salian, S. Mandal, Entropy stabilized multicomponent oxides with diverse functionality–a review, Crit. Rev. Solid State Mater. Sci. 47 (2022) 142–193.

[72] M. Fracchia, M. Coduri, P. Ghigna, U. Anselmi-Tamburini, Phase stability of high entropy oxides: A critical review, J. Eur. Ceram. Soc. (2023).

[73] Y.-J. Deng, V. Tripkovic, J. Rossmeisl, M. Arenz, Oxygen reduction reaction on Pt overlayers deposited onto a gold film: ligand, strain, and ensemble effect, ACS Catal. 6 (2016) 671–676.

[74] Y. Yao, Z. Liu, P. Xie, Z. Huang, T. Li, D. Morris, Z. Finfrock, J. Zhou, M. Jiao, J. Gao, Computationally aided, entropy-driven synthesis of highly efficient and durable multi-elemental alloy catalysts, Sci. Adv. 6 (2020) eaaz0510.

[75] Y. Zhang, T.T. Zuo, Z. Tang, M.C. Gao, K.A. Dahmen, P.K. Liaw, Z.P. Lu, Microstructures and properties of high-entropy alloys, Prog. Mater Sci. 61 (2014) 1–93.

[76] R. Wang, Y. Tang, S. Li, Y. Ai, Y. Li, B. Xiao, X. Liu, S. Bai, Effect of lattice distortion on the diffusion behavior of high-entropy alloys, J. Alloy. Compd. 825 (2020) 154099.

[77] D.B. Miracle, O.N. Senkov, A critical review of high entropy alloys and related concepts, Acta Mater. 122 (2017) 448–511.

[78] Y. Jien-Wei, Recent progress in high entropy alloys, Annales De Chimie - Science Des Matériaux 31 (2006) 633–648.

[79] D. Wang, Z. Liu, S. Du, Y. Zhang, H. Li, Z. Xiao, W. Chen, R. Chen, Y. Wang, Y. Zou, S. Wang, Low-temperature synthesis of small-sized high-entropy oxides for water oxidation, J. Mater. Chem. A 7 (2019) 24211–24216.

[80] M. Qin, Q. Yan, Y. Liu, J. Luo, A new class of high-entropy M 3 B 4 borides, J. Adv. Ceram. 10 (2021) 166–172.

[81] M. Qin, Q. Yan, Y. Liu, H. Wang, C. Wang, T. Lei, K.S. Vecchio, H.L. Xin, T. J. Rupert, J. Luo, Bulk high-entropy hexaborides, J. Eur. Ceram. Soc. 41 (2021) 5775–5781.

[82] M. Cui, C. Yang, B. Li, Q. Dong, M. Wu, S. Hwang, H. Xie, X. Wang, G. Wang, L. Hu, High-entropy metal sulfide nanoparticles promise high-performance oxygen evolution reaction, Adv. Energy Mater. 11 (2021) 2002887.

[83] J. Gild, J. Braun, K. Kaufmann, E. Marin, T. Harrington, P. Hopkins, K. Vecchio, J. Luo, A high-entropy silicide:(Mo0. 2Nb0. 2Ta0. 2Ti0. 2W0. 2) Si2, J. Materiomics 5 (2019) 337–343.

[84] T. Jin, X. Sang, R.R. Unocic, R.T. Kinch, X. Liu, J. Hu, H. Liu, S. Dai, Mechanochemical-assisted synthesis of high-entropy metal nitride via a soft urea strategy, Adv. Mater. 30 (2018) 1707512.

[85] H. Xu, Z. Zhang, J. Liu, C.-L. Do-Thanh, H. Chen, S. Xu, Q. Lin, Y. Jiao, J. Wang, Y. Wang, Entropy-stabilized single-atom Pd catalysts via high-entropy fluorite oxide supports, Nat. Commun. 11 (2020) 3908.

[86] X. Lao, X. Liao, C. Chen, J. Wang, L. Yang, Z. Li, J.W. Ma, A. Fu, H. Gao, P. Guo, Pd-Enriched-Core/Pt-enriched-shell high-entropy alloy with face-centred cubic structure for C1 and C2 alcohol oxidation, Angew. Chem. 135 (2023) e202304510.

[87] S. Li, J. Wang, X. Lin, G. Xie, Y. Huang, X. Liu, H.J. Qiu, Flexible solid-state direct ethanol fuel cell catalyzed by nanoporous high-entropy Al-Pd-Ni-Cu-Mo anode and spinel (AlMnCo) 3O4 cathode, Adv. Funct. Mater. 31 (2021) 2007129.

[88] K. Zeng, J. Zhang, W. Gao, L. Wu, H. Liu, J. Gao, Z. Li, J. Zhou, T. Li, Z. Liang, Surface-decorated high-entropy alloy catalysts with significantly boosted activity and stability, Adv. Funct. Mater. 32 (2022) 2204643.

[89] H. Xu, L. Yang, K. Wang, L. Jin, Y. Liu, G. He, H. Chen, Etched high-entropy prussian blue analogues as trifunctional catalysts for water, ethanol, and urea electrooxidation, Inorg. Chem. 62 (2023) 11271–11277.

[90] D. Fan, K. Guo, Y. Zhang, Q. Hao, M. Han, D. Xu, Engineering high-entropy alloy nanowires network for alcohol electrooxidation, J. Colloid Interface Sci. 625 (2022) 1012–1021.

[91] B. Miao, Z.-P. Wu, H. Xu, M. Zhang, Y. Chen, L. Wang, DFT studies on the key competing reaction steps towards complete ethanol oxidation on transition metal catalysts, Comput. Mater. Sci 156 (2019) 175–186.

[92] C. Zhu, S. Fu, Q. Shi, D. Du, Y. Lin, Single-atom electrocatalysts, Angew. Chem. Int. Ed. 56 (2017) 13944–13960.

[93] B. Qiao, A. Wang, X. Yang, L.F. Allard, Z. Jiang, Y. Cui, J. Liu, J. Li, T. Zhang, Single-atom catalysis of CO oxidation using Pt1/FeO x, Nat. Chem. 3 (2011) 634–641.

[94] X.-F. Yang, A. Wang, B. Qiao, J. Li, J. Liu, T. Zhang, Single-atom catalysts: a new frontier in heterogeneous catalysis, Acc. Chem. Res. 46 (2013) 1740–1748.

[95] Q. Zhang, J. Guan, Single-atom catalysts for electrocatalytic applications, Adv. Funct. Mater. 30 (2020) 2000768.

[96] T. Sun, S. Mitchell, J. Li, P. Lyu, X. Wu, J. Pérez-Ramírez, J. Lu, Design of local atomic environments in single-atom electrocatalysts for renewable energy conversions, Adv. Mater. 33 (2021) 2003075.

[97] Y. Wang, H. Su, Y. He, L. Li, S. Zhu, H. Shen, P. Xie, X. Fu, G. Zhou, C. Feng, Advanced electrocatalysts with single-metal-atom active sites, Chem. Rev. 120 (2020) 12217–12314.

[98] J. Su, R. Ge, Y. Dong, F. Hao, L. Chen, Recent progress in single-atom electrocatalysts: concept, synthesis, and applications in clean energy conversion, J. Mater. Chem. A 6 (2018) 14025–14042.

[99] Z. Jin, P. Li, Z. Fang, G. Yu, Emerging electrochemical techniques for probing site behavior in single-atom electrocatalysts, Acc. Chem. Res. 55 (2022) 759–769.

[100] S. Li, A. Guan, H. Wang, Y. Yan, H. Huang, C. Jing, L. Zhang, L. Zhang, G. Zheng, Hybrid palladium nanoparticles and nickel single atom catalysts for efficient electrocatalytic ethanol oxidation, J. Mater. Chem. A 10 (2022) 6129–6133.

[101] H. Wang, H. Zheng, L. Ling, Q. Fang, L. Jiao, L. Zheng, Y. Qin, Z. Luo, W. Gu, W. Song, Pd metallene aerogels with single-atom W doping for selective ethanol oxidation, ACS Nano 16 (2022) 21266–21274.

[102] Y. Yu, Z. Zhu, H. Huang, Surface engineered single-atom systems for energy conversion, Adv. Mater. 2311148 (2024).

[103] S.G. Peera, C. Liu, J. Shim, A.K. Sahu, T.G. Lee, M. Selvaraj, R. Koutavarapu, MXene (Ti3C2Tx) supported electrocatalysts for methanol and ethanol electrooxidation: A review, Ceram. Int. 47 (2021) 28106–28121.

[104] L. Castanheira, W.O. Silva, F.H. Lima, A. Crisci, L. Dubau, F. Maillard, Carbon corrosion in proton-exchange membrane fuel cells: effect of the carbon structure, the degradation protocol, and the gas atmosphere, ACS Catal. 5 (2015) 2184–2194.

[105] N. Macauley, D.D. Papadias, J. Fairweather, D. Spernjak, D. Langlois, R. Ahluwalia, K.L. More, R. Mukundan, R.L. Borup, Carbon corrosion in PEM fuel cells and the development of accelerated stress tests, J. Electrochem. Soc. 165 (2018) F3148–F3160.

[106] J. Ouyang, Applications of carbon nanotubes and graphene for third-generation solar cells and fuel cells, Nano Materials Science 1 (2019) 77–90.

[107] S. Akula, V. Parthiban, S.G. Peera, B. Singh, S. Dhakate, A. Sahu, Simultaneous Co-doping of nitrogen and fluorine into MWCNTs: an in-situ conversion to graphene like sheets and its electro-catalytic activity toward oxygen reduction reaction, J. Electrochem. Soc. 164 (2017) F568.

[108] W.S. Jung, Study on durability of Pt supported on graphitized carbon under simulated start-up/shut-down conditions for polymer electrolyte membrane fuel cells, Journal of Energy Chemistry 27 (2018) 326–334.
[109] S.G. Peera, A. Arunchander, A. Sahu, Platinum nanoparticles supported on nitrogen and fluorine co-doped graphite nanofibers as an excellent and durable oxygen reduction catalyst for polymer electrolyte fuel cells, Carbon 107 (2016) 667–679.
[110] A.N.R. Alfonso, M.L. Villanueva, J.R.P. Laxamana, H.G.G. Necesito, B.J.V. Tongol, Enhanced electrocatalytic activity of palladium electrocatalysts supported on corncob biochar for ethanol oxidation reaction in alkaline medium, J. Chin. Chem. Soc. (2024).
[111] J.J. Ogada, T.J. Ehirim, A.K. Ipadeola, A.B. Haruna, P.V. Mwonga, A.M. Abdullah, X.-Y. Yang, K. Eid, D.M. Wamwangi, K.I. Ozoemena, Interfacial Electronic Interactions within the Pd-CeO2/Carbon Onions Define the Efficient Electrocatalytic Ethanol Oxidation Reaction in Alkaline Electrolytes, ACS Omega 9 (2024) 7439–7451.
[112] C. Xia, H. Ye, A. Kim, A.S. Namini, S. Li, S.A. Delbari, J.Y. Park, D. Kim, Q. Van Le, R.S. Varma, Recent catalytic applications of MXene-based layered nanomaterials, Chemosphere 931 (2023) 138323.
[113] C. Xia, H. Ye, A. Kim, A. Sabahi Namini, S. Li, S. A. Delbari, J. Y. Park, D. Kim, Q. V. Le, R. S. Varma, R. Luque, T. R. A, H. W. Jang, and M. Shokouhimehr, "Recent catalytic applications of MXene-based layered nanomaterials," *Chemosphere,* 325 (2023) 138323.
[114] W. Peng, J. Zhou, Y.R. Lu, M. Peng, D. Yuan, T.S. Chan, Y. Tan, Palladium metallene confined on MXene with increased hydroxyl binding strength for highly efficient ethanol electrooxidation, PNAS 120 (2023) e2222096120.
[115] P.P. Patel, M.K. Datta, P.H. Jampani, D. Hong, J.A. Poston, A. Manivannan, P. N. Kumta, High performance and durable nanostructured TiN supported Pt50–Ru50 anode catalyst for direct methanol fuel cell (DMFC), J. Power Sources 293 (2015) 437–446.
[116] J. Peng, X. Chen, W.-J. Ong, X. Zhao, N. Li, Surface and heterointerface engineering of 2D MXenes and their nanocomposites: insights into electro-and photocatalysis, Chem 5 (2019) 18–50.
[117] J. Zhang, Y. Zhao, X. Guo, C. Chen, C.-L. Dong, R.-S. Liu, C.-P. Han, Y. Li, Y. Gogotsi, G. Wang, Single platinum atoms immobilized on an MXene as an efficient catalyst for the hydrogen evolution reaction, Nat. Catal. 1 (2018) 985–992.
[118] V.M.H. Ng, H. Huang, K. Zhou, P.S. Lee, W. Que, J.Z. Xu, L.B. Kong, Recent progress in layered transition metal carbides and/or nitrides (MXenes) and their composites: synthesis and applications, J. Mater. Chem. A 5 (2017) 3039–3068.
[119] Z. Chen, B. Yu, J. Cao, X. Wen, M. Luo, S. Xing, D. Chen, C. Feng, G. Huang, Y. Jin, High-performance Pd nanocatalysts based on the novel N-doped Ti3C2 support for ethanol electrooxidation in alkaline media, Electrochim. Acta 390 (2021) 138902.
[120] Z. Chen, F. Jing, M. Luo, X. Wu, H. Fu, S. Xiao, B. Yu, D. Chen, X. Xiong, Y. Jin, Local coordination and electronic interactions of Pd/MXene via dual-atom codoping with superior durability for efficient electrocatalytic ethanol oxidation, Carbon Energy (2024).
[121] S. Li, L. Zhao, J. Shu, H. Niu, R. Li, J. Zhao, H. Yang, J. Jin, R. Jin, Mxene coupled over nitrogen-doped graphene anchoring palladium nanocrystals as an advanced electrocatalyst for the ethanol electrooxidation, Journal of Colloid Interface Science 610 (2022) 944–952.
[122] M. Naguib, O. Mashtalir, J. Carle, V. Presser, J. Lu, L. Hultman, Y. Gogotsi, M. W. Barsoum, Two-dimensional transition metal carbides, ACS Nano 6 (2012) 1322–1331.
[123] P. Wang, H. Cui, C. Wang, In situ formation of porous trimetallic PtRhFe nanospheres decorated on ultrathin MXene nanosheets as highly efficient catalysts for ethanol oxidation, Nano Energy 66 (2019) 104196.
[124] J. Cao, X. Wu, Y. Chen, Z. Chen, R. Jiang, Y. Zhao, Q. Tian, D. Chen, S. Xiao, B. Yu, Y. Jin, Electronic regulation over Pd nanoparticles: One-pot synthesis of B, N Co-doping MXene-supported Pd catalyst for efficient ethanol oxidation, J. Alloy. Compd. 955 (2023) 170240.
[125] S. Choung, W. Park, J. Moon, J.W. Han, Rise of machine learning potentials in heterogeneous catalysis: Developments, applications, and prospects, Chem. Eng. J. 494 (2024) 152757.
[126] X. Liu, H.-J. Peng, Toward Next-Generation Heterogeneous Catalysts: Empowering Surface Reactivity Prediction with Machine Learning, Engineering (2024).
[127] C. Cheng, X. Zhang, Z. Fu, Z. Yang, Strong metal–support interactions impart activity in the oxygen reduction reaction: Au monolayer on Mo2C (MXene), J. Phys. Condens. Matter 30 (2018) 475201.
[128] X. Yang, Y. Zhang, Z. Fu, Z. Lu, X. Zhang, Y. Wang, Z. Yang, R. Wu, Tailoring the electronic structure of transition metals by the V2C MXene support: excellent oxygen reduction performance triggered by metal–support interactions, ACS Appl. Mater. Interfaces 12 (2020) 28206–28216.